

Benchmarking a fading window: electroweak baryogenesis in the C2HDM, LHC constraints after Run 2 and prospects for LISA

Thomas Biekötter^{1,*} and María Olalla Olea-Romacho^{2,†}

¹*Instituto de Física Teórica UAM/CSIC, Calle Nicolás Cabrera 13-15, Cantoblanco, 28049, Madrid, Spain*

²*Theoretical Particle Physics and Cosmology, King's College London, Strand, London WC2R 2LS, United Kingdom*

The origin of the baryon asymmetry of the universe remains one of the most pressing open questions in particle physics and cosmology. Electroweak baryogenesis offers an experimentally testable explanation, requiring new sources of CP violation and a strong first-order electroweak phase transition. The Two Higgs doublet model (2HDM) is the simplest scalar extension of the Standard Model that can accommodate both ingredients. We critically assess the viability of the complex 2HDM (C2HDM) (a 2HDM with a softly broken \mathbb{Z}_2 symmetry and a single source of explicit CP violation in the Higgs sector) as a framework for electroweak baryogenesis, incorporating for the first time a comprehensive set of LHC Run 2 results at 13 TeV. By defining CP-violating benchmark planes tailored for a strong first-order electroweak phase transition, we identify regions of parameter space motivated by electroweak baryogenesis that will be testable at the LHC, and at future space-based gravitational wave experiments. The benchmark planes are intended to guide ongoing efforts in defining representative scenarios for the exploration of CP-violation in extended scalar sectors at the LHC Run 3 and beyond, while also assessing the emerging synergy between the LHC and future gravitational wave observatories such as LISA. We also quantify the current tension between the realisation of electroweak baryogenesis and the non-observation of the electron electric dipole moment (EDM), finding that the predicted electron EDMs typically exceed the experimental limits by at least an order of magnitude.

I. INTRODUCTION

The origin of the cosmic matter–antimatter asymmetry remains one of the most compelling open problems in fundamental physics. This asymmetry can be quantified in terms of the observed baryon-to-photon ratio [1]

$$\eta_\gamma \approx 6.14 \times 10^{-10}. \quad (1)$$

A dynamical explanation of this baryon asymmetry of the universe (BAU) requires the three Sakharov conditions to be fulfilled: violation of baryon number, violation of C and CP symmetry, and a significant departure from thermal equilibrium [2]. While the Standard Model (SM) contains ingredients that satisfy the Sakharov conditions, such as baryon number violating processes via electroweak (EW) sphalerons [3, 4] and CP violation through the complex phase in the CKM matrix, it fails to generate a sufficient BAU. For a Higgs boson mass of 125 GeV, the EW phase transition (EWPT) is a smooth crossover rather than a strong first-order EWPT [5], thereby failing the required departure-from-equilibrium condition. Furthermore, even under the presence of a sufficiently strong EWPT, the CP violation contained in the SM is far too small to produce the observed BAU [6].

The shortcoming of the SM to explain the BAU has motivated many extensions of the Higgs sector aimed at realising EW baryogenesis (EWBG) [4]. The simplest and most studied scenario that can realise EWBG is the two Higgs doublet model (2HDM) [7]. By introducing a second Higgs doublet, the 2HDM can substantially alter the EW symmetry-breaking dynamics and provide additional CP-violating phases beyond the CKM matrix in the Higgs sector. It has long been known that 2HDMs can accommodate a strong first-order EWPT [8–21], for example, through relatively large mass splittings between the additional Higgs bosons predicted by the model [10, 15, 22, 23]. However, the parameter space that enables successful EWBG in the 2HDM is increasingly under pressure from experimental observations. The non-decoupling effects required to generate a sufficiently strong EWPT prefer a light spectrum of the additional Higgs bosons not too far beyond the EW scale, making the EWPT a collider target [24]. Accordingly, the non-observation of beyond the SM (BSM) Higgs bosons at the Large Hadron collider (LHC) are able to exclude large parts of the parameter space [25, 26], in particular the regions of parameter space suitable for EWBG [16, 19].

This is especially true for the searches performed during the LHC Run 2 at an unprecedented center-of-mass energy of 13 TeV, where novel signatures including the production of more than one BSM Higgs boson have been considered. In this paper, we will for the first time confront the parameter regions favoured by EWBG in the complex 2HDM (C2HDM) [27, 28], the CP-violating 2HDM with softly-broken \mathbb{Z}_2 symme-

* thomas.biekoetter@desy.de

† maria.olalla.olea-romacho@kcl.ac.uk

try, with a comprehensive set of cross section limits from LHC searches performed at 13 TeV using the public code `HiggsTools` [29, 30]. This will allow us to define benchmark planes for the C2HDM that are compatible with current LHC constraints. These benchmark planes are intended to guide the ongoing efforts in defining representative scenarios for the exploration of CP-violation in extended scalar sectors at the LHC Run 3 and beyond. We will focus on benchmark planes tailored for a strong EWPT, identifying regions of parameter space suitable for EWBG that will be further probed in future Runs of the LHC.

In addition to assessing the experimental viability of these regions in light of LHC Run 2 results at 13 TeV, we examine whether they could lead to complementary signals at future space-based gravitational wave (GW) detectors such as LISA [10, 17, 31]. GW from a strong first-order EWPT are often highlighted as a key signature of EWBG. We will show that there are regions of parameter space that are compatible both with EWBG and with GW signals that are detectable with LISA. However, in most parts of the parameter space regions favoured by EWBG, the predicted signal-to-noise ratios (SNRs) lie below LISA’s sensitivity threshold, posing a challenge for detection [19]. Here it is important to note that the theoretical uncertainties in the prediction of the parameters characterizing the EWPT suffer from sizable theoretical uncertainties [32–34]. These uncertainties translate into substantial uncertainties in the predictions for the BAU and the GW signals, such that the actual prospects for detection could be somewhat more optimistic than our estimates suggest.

Some of the benchmark planes that we are proposing are motivated by studies of the EWPT performed in the real 2HDM (R2HDM), where the Higgs sector is assumed to conserve the CP symmetry. Studies in the R2HDM have shown that a large separation between a heavier new CP-odd Higgs boson A and a lighter new CP-even Higgs boson H facilitates the strongest EWPTs [11, 22, 23]. An important consequence is that this mass hierarchy allows kinematically for the decay $A \rightarrow ZH$. This signature has consequently been dubbed a “smoking gun” signature of a strong first-order EWPT in the 2HDM [10, 23, 35] since the same physics (a large coupling and mass gap) that facilitates a strong EWPT, also increases the cross sections for the $A \rightarrow ZH$ signal [23, 36]. We will demonstrate here with a selection of benchmark scenarios that the C2HDM inherits this phenomenology, with sizable mass gaps between the BSM neutral scalars facilitating the strongest transitions, and we study the impact of the CP violation in the Higgs sector on the strength of the EWPT in such scenarios. Moreover, we will analyse which additional collider signatures play a role in the C2HDM that can probe parameter regions with a strong EWPT, which are not present in the R2HDM.

We also present a benchmark plane in which a strong EWPT is realised without large mass splittings between the BSM scalars, such that the decay $A \rightarrow ZH$ is ab-

sent. This possibility requires small values of $\tan \beta$ (defined as the ratio of the vacuum expectation values (vev) of the two Higgs doublets) and an overall lighter spectrum [12, 14]. While we give an explicit example of such a scenario that remains compatible with existing limits from LHC searches, we will argue that this possibility is on the verge of being excluded. Accordingly, there are good prospects for finally excluding (or confirming, e.g. via the detection of the charged scalars) this scenario during Run 3. We also find that the EWPT in almost mass degenerate scenarios is substantially smaller, barely satisfying the baryon number preservation condition [4, 37] that prohibits the washout of the BAU after the transition. In addition, the smaller strengths of the EWPT in this scenario gives rise to GWs with LISA SNRs of the order of 10^{-8} or below, such that it is unlikely that it can be probed with LISA.

Another key challenge for EWBG that has emerged in recent years is that scenarios with new sources of CP violation are stringently constrained by experimental limits on electric dipole moments (EDMs), in particular the electron EDM [38, 39]. In the C2HDM, the same CP-violating phase responsible for generating the BAU also induces an electron EDM at the two-loop level via Barr–Zee-type diagrams that typically is substantially larger than the experimental upper bounds [26]. As such, the non-observation of an EDM places strong pressure on the parameter space relevant for EWBG. In this work, we compute the predicted electron EDMs across our benchmark scenarios, but we do not impose the experimental bounds as a hard constraint. Instead, we indicate the electron EDM values on our benchmark planes in order to quantify the level of tension. This approach reflects the possibility that the electron EDM may be suppressed in more general extensions of the C2HDM, e.g. via additional CP-violating phases (if hard breaking of the \mathbb{Z}_2 symmetry is considered) [18] or novel mechanisms such as secluded [40] or transient [41] CP violation, without affecting the dynamics of the EWPT.

Taking into account both the new LHC Run 2 results at 13 TeV and the non-observation of the electron EDM, our findings suggest that the C2HDM may face challenges as a benchmark model for EWBG. In addition, only a small part of the parameter region suitable for EWBG produces GW signals that are strong enough to be detectable with LISA. Nevertheless, our benchmark planes reveal that interesting parameter regions still persist, some of which can serve as well-motivated benchmark scenarios for future LHC searches, and a subset even includes regions where successful EWBG is accompanied by GW signals within LISA’s projected sensitivity.

II. THE 2HDM

In this section, we briefly introduce the 2HDM and establish our notation, beginning with the CP-conserving R2HDM. Although our primary focus lies on the CP-

violating C2HDM, starting from the CP-conserving case allows us to point out more transparently the differences in the dynamics of the EWPT and the role of CP violation in our numerical analysis.

A. The real two-Higgs-doublet model

In this section, we present a short overview of the CP-conserving R2HDM. The Higgs sector consists of two SU(2) Higgs doublets, Φ_1 and Φ_2 , both carrying hypercharge $1/2$.¹ The doublets can be written in terms of their neutral and charged components

$$\Phi_1 = \begin{pmatrix} \phi_1^+ \\ (\phi_1 + i\sigma_1)/\sqrt{2} \end{pmatrix}, \quad \Phi_2 = \begin{pmatrix} \phi_2^+ \\ (\phi_2 + i\sigma_2)/\sqrt{2} \end{pmatrix}. \quad (2)$$

To suppress tree-level flavor-changing neutral currents, we impose a softly broken \mathbb{Z}_2 symmetry [43, 44] under which the Higgs doublets transform as $\Phi_1 \rightarrow \Phi_1$ and $\Phi_2 \rightarrow -\Phi_2$, and which extends to the Yukawa sector, see below. At tree level, the scalar potential takes the form

$$\begin{aligned} V_{\text{tree}}(\Phi_1, \Phi_2) = & \quad (3) \\ & m_{11}^2 \Phi_1^\dagger \Phi_1 + m_{22}^2 \Phi_2^\dagger \Phi_2 - (m_{12}^2 \Phi_1^\dagger \Phi_2 + \text{h.c.}) \\ & + \frac{1}{2} \lambda_1 (\Phi_1^\dagger \Phi_1)^2 + \frac{1}{2} \lambda_2 (\Phi_2^\dagger \Phi_2)^2 + \lambda_3 (\Phi_1^\dagger \Phi_1)(\Phi_2^\dagger \Phi_2) \\ & + \lambda_4 (\Phi_1^\dagger \Phi_2)(\Phi_2^\dagger \Phi_1) + \frac{1}{2} (\lambda_5 (\Phi_1^\dagger \Phi_2)^2 + \text{h.c.}). \end{aligned}$$

where all parameters are real, ensuring CP-conservation. The vacuum expectation values (vevs) of the Higgs doublets are given by $\langle \phi_1 \rangle = v_1$ and $\langle \phi_2 \rangle = v_2$, satisfying the relation $v_1^2 + v_2^2 \equiv v^2 \approx 246$ GeV, with the ratio of vevs parameterized as $\tan \beta \equiv t_\beta = v_2/v_1$.

After electroweak symmetry breaking, the R2HDM predicts five physical Higgs states: two neutral CP-even scalars h and H , one neutral CP-odd pseudoscalar A , and a pair of charged Higgs bosons H^\pm . The transition from the gauge basis to the mass basis is governed by two mixing angles: α for the CP-even sector and β for the CP-odd/charged sector. The lighter CP-even state h is conventionally identified as the observed Higgs boson [45, 46] at $m_h = 125$ GeV. The *alignment limit* is defined by [47]

$$\cos(\beta - \alpha) = 0, \quad (4)$$

where the couplings of h match those of the SM Higgs boson at tree level.

Since Φ_1 and Φ_2 transform differently under the \mathbb{Z}_2 symmetry, each fermion type can only couple to one of the Higgs doublets. This results in four different 2HDM types, depending on how the \mathbb{Z}_2 symmetry is assigned

in the Yukawa sector. For our benchmark planes, we focus on the type I where all fermions couple to the Higgs doublet Φ_2 , as it is the least constrained by current LHC data among the four types. In particular, it allows for the largest deviations from the alignment limit without conflicting with measurements of the 125 GeV Higgs boson [30, 31]. Notably, in the exact alignment limit, the direct production of the additional neutral and charged scalars is suppressed with increasing t_β , thereby evading many of the existing constraints from searches for these particles.

Although our analysis is performed within the C2HDM, it is useful to define the set of input parameters of the R2HDM, as this facilitates a transparent comparison in the CP-conserving limit where (in our parameter basis of the C2HDM, see below) the C2HDM smoothly reduces to the real 2HDM. The 2HDM parameter space can be most conveniently investigated with the following set of input parameters,

$$t_\beta, M, v, \cos(\beta - \alpha), m_h, m_H, m_A, m_{H^\pm}, \quad (5)$$

where we defined the \mathbb{Z}_2 -breaking scale

$$M^2 = \frac{m_{12}^2}{s_\beta c_\beta}, \quad (6)$$

and where $v \approx 246$ GeV and $m_h \approx 125$ GeV are fixed from experimental input.

B. The complex two-Higgs-doublet model

Analogous to the R2HDM, the tree-level scalar potential of the C2HDM is constructed from two SU(2)_L scalar doublets, Φ_1 and Φ_2 , both carrying a hypercharge of $1/2$, as shown in Eq. (2). The scalar potential has the same form as in Eq. (3), respecting a \mathbb{Z}_2 symmetry only softly broken by the term proportional to m_{12}^2 , but now allowing m_{12}^2 and λ_5 to take complex values [27, 28]. Without loss of generality, we work in a basis in which at zero temperature the vevs of the neutral components of the Higgs doublets are real and positive numbers, i.e. $\langle \phi_1 \rangle = v_1$ and $\langle \phi_2 \rangle = v_2$ [9]. This promotes $t_\beta = v_1/v_2$ to a physical parameter once a specific Yukawa type is chosen [48]. For the discussion of the EWPT in Section IID, we note that at finite temperature T , the Higgs doublets can develop CP-violating and charge-breaking vevs v_{CP} and v_{CB} , respectively. Then, the most general vacuum can be written as

$$\langle \Phi_1(T) \rangle = \begin{pmatrix} 0 \\ v_1(T) \end{pmatrix}, \quad \langle \Phi_2(T) \rangle = \begin{pmatrix} v_{\text{CB}}(T) \\ v_2(T) + i v_{\text{CP}}(T) \end{pmatrix}, \quad (7)$$

with $v_{\text{CP}}(T=0) = v_{\text{CB}}(T=0) = 0$.

In contrast to the R2HDM, the C2HDM allows for explicit CP violation through complex parameters in the scalar potential. Making use of a global rephasing invariance and the freedom to perform phase rotations of

¹For a comprehensive review of the 2HDM, see e.g. Ref. [42].

the Higgs doublets [28, 49], only one independent complex phase remains. All parameters can be taken real except for the soft \mathbb{Z}_2 -breaking term m_{12}^2 and the quartic coupling λ_5 , whose complex phases are related by

$$\text{Im}(m_{12}^2) = \frac{1}{2} s_\beta c_\beta v^2 \text{Im}(\lambda_5), \quad (8)$$

expressing the fact that there is only one independent CP-violating phase in the model.

The physical spectrum after EW symmetry breaking consists of three neutral scalars h_1 , h_2 , and h_3 , which are, in general, admixtures of CP eigenstates. In what follows, we assume a mass ordering given by $m_{h_1} = 125 \text{ GeV} < m_{h_2} < m_{h_3}$, along with a pair of charged Higgs bosons H^\pm with mass m_{H^\pm} . The rotation from the interaction basis ϕ_1, ϕ_2 and $A = -s_\beta \sigma_1 + c_\beta \sigma_2$ to the mass eigenstate basis $h_{1,2,3}$ can be expressed via a 3×3 orthogonal rotation matrix R_{ij} , which we parametrise using the three mixing angles α_1, α_2 , and α_3 ,

$$R = \begin{pmatrix} c_1 c_2 & s_1 c_2 & s_2 \\ -(c_1 s_2 s_3 + s_1 c_3) & c_1 c_3 - s_1 s_2 s_3 & c_2 s_3 \\ -c_1 s_2 c_3 + s_1 s_3 & -(c_1 s_3 + s_1 s_2 c_3) & c_2 c_3 \end{pmatrix}, \quad (9)$$

with the shorthand notation $s_i = \sin \alpha_i$, $c_i = \cos \alpha_i$, ($i = 1, 2, 3$). The admixture of the states $\phi_{1,2}$ with the state A signals CP violation, whereas in the CP-conserving limit, e.g. $\alpha_2 = \alpha_3 = 0$, the mixing matrix R decomposes into a block diagonal form with a 2×2 matrix rotating the fields $\phi_{1,2}$ into two CP-even mass eigenstates, and the field A becomes a CP-odd mass eigenstate. As discussed above, there is only one independent CP-violating phase in the C2HDM. However, both angles α_2 and α_3 parametrise the CP-violating mixing in the neutral scalar sector. As a consequence, in the C2HDM it is not possible to use all physical scalar masses and all mixing angles as independent input parameters, in contrast to the real 2HDM as shown in Eq. (5). Different strategies have been adopted in the literature to define a set of input parameters. One common approach is to use all three mixing angles $\alpha_{1,2,3}$ as free parameters, in which case only two of the three neutral scalar masses can be kept as free parameters, and one is a dependent parameter (see, e.g. Refs. [14, 16, 25, 26, 50]). However, this parametrisation makes it impossible to study benchmark planes with all physical masses kept fixed, which is useful to isolate the impact of CP violation on the dynamics of the EWPT, which we want to investigate here. Moreover, in general it does not allow to continuously approach the CP-conserving limit because the predicted mass can become tachyonic.

We therefore use a different parametrisation in which only the two mixing angles α_1 and α_3 are independent input parameters, whereas α_2 is a derived parameter. Similar parameterizations of the C2HDM with slightly different notations have been used in the past in the context of EWBG in Refs. [19, 51–53]. In total, we use the following set of input parameters to define our benchmark

planes,

$$t_\beta, M, v, \alpha_1, \alpha_3, m_{h_1}, m_{h_2}, m_{h_3}, m_{H^\pm}, \quad (10)$$

where the \mathbb{Z}_2 -breaking scale in the C2HDM is defined by

$$M^2 = \frac{\text{Re}(m_{12}^2)}{s_\beta c_\beta}. \quad (11)$$

The set of equations that relates this set of parameters to the parameters of the potential shown in Eq. (16) are given in Appendix A. In this parametrisation, the angle α_1 acts as a parameter quantifying departures from the C2HDM alignment limit. Under the presence of small CP-odd components in the SM-like Higgs boson h_1 (e.g. $\alpha_3 \approx 0$, see discussion below) as required in the Yukawa type I to be compatible with LHC data [25], the alignment limit in the C2HDM can be approximately defined by

$$s_{\beta-\alpha_1} \equiv \sin(\beta - \alpha_1) \approx 0, \quad (12)$$

such that $\alpha_1 \neq \beta$ signal departures from the alignment limit.² The angle α_3 acts as a parametrisation of the amount of CP violation. The CP-conserving limit is achieved for either $\alpha_3 \rightarrow 0$, for which h_2 becomes a pure CP-even state corresponding to the state H of the real 2HDM and h_3 becomes a CP-odd state corresponding to the state A of the real 2HDM, or $\alpha_3 \rightarrow \pm\pi/2$, for which conversely h_2 and h_3 correspond to the states A and H , respectively. In both cases, the derived parameter α_2 vanishes.

C. Theoretical and experimental constraints

All benchmark planes defined in this work satisfy the following set of theoretical and experimental constraints.

1. Theoretical constraints

On the theory side, we ensure absolute stability of the EW vacuum for all points featuring a strong EWPT using the public code **BSMPT v.3** [54–56]. To this end, we verify that the effective potential at one-loop level and zero temperature (see the discussion in Section IID) is bounded from below and that the minimum corresponding to the EW vacuum is the global minimum of the potential. Near the alignment limit, the bounded-from-below conditions are most naturally satisfied by requiring $M \leq m_{h_2}, m_{h_3}, m_{H^\pm}$, a condition we impose throughout to define the benchmark planes.

²Due to different conventions for defining the rotation matrices, the alignment limit in the C2HDM is defined with the sine, whereas the alignment limit in the real 2HDM is typically defined with the cosine, see Eq. (4).

We note that, for a subset of parameter points featuring a strong EWPT and a stable EW vacuum at one-loop level, the tree-level scalar potential is unbounded from below. While this does not constitute an inconsistency (since quantum corrections can indeed stabilise or destabilise the potential) it implies that the vacuum stability of these points relies on the one-loop contributions. This introduces a degree of theoretical uncertainty, as corrections from higher orders could, in principle, alter the stability of the vacuum again. We find that the boundary between parameter space regions with a bounded and unbounded potential shifts only slightly between the tree-level and one-loop analyses. To maintain clarity in our presentation, we do not indicate tree-level bounded-from-below exclusions in the plots, as this would in general be too restrictive [57]. Importantly, we have verified that the vast majority of these points lie in regions already excluded by current LHC searches, as discussed in Section II C 4, such that this issue does not have an impact on our conclusions regarding the possibility to realise EWBG or predict GW signals potentially detectable with LISA.

To ensure perturbativity, we use the public code **ScannerS v.2** [58] to test each parameter point against leading-order perturbative unitarity constraints in the high-energy limit [59], ensuring that, if not indicated otherwise, the whole benchmark planes lie within the perturbative regime. These conditions place upper bounds on the absolute values of the quartic scalar couplings λ_i , which govern both the mass splitting between the \mathbb{Z}_2 -breaking scale M and the BSM scalar masses, as well as the mass differences among the BSM states themselves. As a result, perturbative unitarity conditions exclude parameter regions where the difference among the parameters M , m_{h_2} , m_{h_3} and m_{H^\pm} are substantially larger than $v \approx 246$ GeV.

2. EW precision observables

On the experimental side, we make sure that our benchmark planes are compatible with constraints from EW precision observables in the form of the oblique parameters S , U and T [60]. Close to the alignment limit and with small CP-violating mixing in the scalar sector, these constraints can be satisfied if at least one of the BSM neutral state h_2 or h_3 is approximately mass degenerate with the charged scalars m_{H^\pm} [61]. Under the presence of large CP-violating mixing between h_2 and h_3 , the constraints on the EW precision observables can be most easily satisfied if all BSM states are approximately mass degenerate.

3. Flavour-physics observables

Further indirect constraints on the C2HDM parameter space arise from flavour-physics observables. In partic-

ular, measurements of radiative B -meson decays in the form of $\bar{B} \rightarrow X_s \gamma$ transitions and of leptonic B -meson decays from $B^0 \rightarrow \mu^+ \mu^-$ decays provide fairly robust lower limits on t_β . We have verified using the public code **thdmTools v.1.3** [23], interfaced with **SuperIso v.4.1** [62, 63], that current experimental results [64–66] exclude values of $t_\beta \lesssim 1.5$ at approximately the 2σ level for charged Higgs boson masses in the range $400 \text{ GeV} \lesssim m_{H^\pm} \lesssim 800 \text{ GeV}$, across all Yukawa types. Thus, for our benchmark planes in type I we use values of $t_\beta \geq 1.5$. For the type II and the flipped type, the constraints from $\bar{B} \rightarrow X_s \gamma$ transitions give rise to an additional lower limit of $m_{H^\pm} \gtrsim 500 \text{ GeV}$ [25, 67].³

4. LHC searches

Regarding collider constraints, we incorporate the latest LHC results from searches for additional Higgs bosons and from cross-section measurements of the 125 GeV Higgs boson using the public tool **HiggsTools v. 1.2** [30]. In this way we can include for the first time a comprehensive set of LHC Run 2 results at 13 TeV in an analysis of the EWPT in the C2HDM, while in previous studies of the EWPT in the C2HDM (and extensions thereof) the wealth of new final states explored during Run 2 was not yet included [16, 19, 68, 69]. **HiggsTools** enables us to include a wide range of dedicated searches for additional Higgs bosons, many of which are particularly sensitive to CP-violating scenarios. Since our goal is to provide benchmark planes as a road map for future LHC searches, it is crucial to verify that the corresponding parameter regions are compatible with the already existing limits.

LHC searches that become especially relevant under the presence of CP violation in the C2HDM include searches for a heavy spin-0 resonance X decaying into Zh , where h is SM-like Higgs boson at 125 GeV [70, 71]. While in the C2HDM the state X can be either h_2 or h_3 (if kinematically allowed), in the CP-conserving 2HDM only the decay $A \rightarrow Zh$ is allowed at tree level, whereas $H \rightarrow Zh$ is forbidden. The presence of two scalars, h_2 and h_3 , potentially decaying into the 125 GeV Higgs boson and a Z -boson makes the Zh final state exceptionally important [25, 53, 72]. We will also discuss the impact of these searches in comparison to the smoking-gun signature $A \rightarrow ZH$ from the R2HDM, with the heavier CP-even BSM state H in the final state, see the discussion in Section I. This process and its role in probing the

³Three of the four benchmark planes presented below feature values of $m_{H^\pm} \geq 650 \text{ GeV}$, such that they satisfy the constraints from $\bar{B} \rightarrow X_s \gamma$ transitions in all Yukawa types and not only in the type I considered here. The final benchmark plane with an almost mass degenerate spectrum and $m_{H^\pm} = 400 \text{ GeV}$ would be in tension with this constraint in type II and the flipped Yukawa type.

EWPT in the R2HDM has been extensively discussed in previous works [22, 23, 36], and we will here focus on its impact in the C2HDM.

In addition, the increased mass reach of Run 2 at 13 TeV allows for probing a richer Higgs-boson pair-production phenomenology. Searches for the pair-production of the 125 GeV Higgs boson have become a central part of the future LHC Higgs-physics programme [73, 74]. In the C2HDM, h_1 -pairs can be resonantly produced by both $h_2 \rightarrow h_1 h_1$ and $h_3 \rightarrow h_1 h_1$ decays if kinematically allowed. On the other hand, the CP-conserving 2HDM only allows for the decay $H \rightarrow hh$, whereas $A \rightarrow hh$ is forbidden. With the 13 TeV data collected during Run 2, ATLAS and CMS also reported for the first time results from searches for a heavy spin-0 resonance X decaying into a SM-like Higgs boson and another lighter new spin-0 resonance Y [75, 76].⁴ If kinematically allowed, in the C2HDM this $X \rightarrow hY$ channel is in general realised via $h_3 \rightarrow h_1 h_2$ decays irrespective of the precise CP-admixtures of the states h_i . On the contrary, there is no hHA -coupling in the R2HDM, such that searches for $X \rightarrow hY$ with $m_Y \neq 125$ GeV cannot probe the R2HDM. In addition to becoming more relevant in the presence of CP violation [50], such multi-scalar signatures are also increasingly important in the context of EWPTs, as they are governed by triple-scalar couplings that directly probe the shape of the scalar potential, potentially providing crucial information about the dynamics of the transition.

In addition to the novel signatures discussed above, also the traditional search channels for a Higgs boson decaying (depending on the mass range) into pairs of massive gauge bosons or third-generation fermions are affected by the presence of CP violation. For example, in the R2HDM the CP-odd state A does not couple at tree level to gauge bosons, such that its decays into WW and ZZ are highly suppressed, and only the decays $H \rightarrow WW$ and $H \rightarrow ZZ$ are promising. In the C2HDM, outside of the alignment limit both h_2 and h_3 can decay into massive gauge bosons with sizable rates, giving rise to stronger constraints especially for masses below the di-top threshold [80]. Finally, above the di-top threshold, searches for heavy Higgs bosons decaying into $t\bar{t}$ pairs exclude small t_β -values of $t_\beta \approx 1$ in the CP-conserving 2HDM [81]. A CP-violating mixing between heavy states h_2 and h_3 can yield interesting signal-signal interference patterns in the $m_{t\bar{t}}$ invariant mass distributions [82] which have not been explored experimentally yet. Instead, in the C2HDM, the low- t_β region can currently constrain more robustly in final states with four top quarks [83, 84], which is much less sensitive to signal-background and signal-signal interference effects.

Finally, it is known that the regions with a strong

EWPT in the 2HDM are correlated with sizable radiative enhancements of the 125 GeV Higgs boson self-coupling by about 50 to 150% [14, 85]. In particular, parameter points featuring an EWPT strong enough to source a GW signal potentially detectable at LISA predict values of $\kappa_\lambda \approx 2$ [22], where κ_λ is the hhh -coupling normalized to the SM leading-order prediction. At the LHC, the Higgs boson self-coupling is directly accessible via non-resonant Higgs boson pair production. Due to destructive interference effects, the enhancements of the self-coupling yield a suppression of the total cross section for hh -production at the LHC. Current upper limits on κ_λ are at the level of $\kappa_\lambda \lesssim 7$ at 95% confidence level [86, 87]. Thus, the measurements of the Higgs boson self-coupling are currently still far from probing models featuring a strong EWPT. We therefore do not focus on constraints on the Higgs boson self-coupling in our discussion. However, the projected sensitivity from the high-luminosity LHC indicates that it will be possible to set a limit of $\kappa_\lambda < 1.6$ at 95% confidence level [88]. Accordingly, during the high-luminosity stage, the LHC is expected to be able to probe the parameter space regions with the strongest EWPT in the 2HDM via non-resonant Higgs boson pair production.

5. Electron EDM

New sources of CP violation can be constrained with measurements of EDMs. For simplicity, we focus exclusively on the electron EDM, as it provides the most robust and model-independent constraint on new CP-violating phases in the Higgs sector. In our analysis, we compute the EDM of the electron at the two-loop level using Barr–Zee-type diagrams [89], as implemented in the public code **ScannerS** v.2 [58]. In the absence of suppression mechanisms, heavy new physics with CP-violating interactions generates an electron EDM that roughly scales via [90]

$$|d_e| \sim \frac{m_e}{1 \text{ MeV}} \left(\frac{1 \text{ TeV}}{M_{\text{UV}}} \right)^2 \cdot 10^{-26} e \text{ cm}, \quad (13)$$

where M_{UV} represents the mass scale of the particles whose interactions are CP-violating, and m_e is the electron mass. In the C2HDM, with new Higgs bosons at the EW scale, one therefore expects to find values of the order of $|d_e| \sim 10^{-28} e \text{ cm}$. The theoretical predictions can be compared to the current experimental upper bounds set by the ACME collaboration in 2018 [38],

$$|d_e| < 1.1 \cdot 10^{-29} e \text{ cm} \quad \text{at 90\% CL}, \quad (14)$$

and the JILA collaborations in 2022s [39],

$$|d_e| < 4.1 \cdot 10^{-30} e \text{ cm} \quad \text{at 90\% CL}, \quad (15)$$

These are the most stringent limits on new sources of CP violation to date. The experimental upper limits

⁴There are further very recent results by CMS [77, 78] and ATLAS [79] that are not yet included in **HiggsTools** and therefore not taken into account here.

are about two orders of magnitude below the values suggested by the scaling argument discussed above, demonstrating the current tension between C2HDM predictions and the non-observation of an electron EDM. In principle, it is possible to fine-tune the parameters of the C2HDM so that different two-loop contributions to the electron EDM interfere destructively, thereby reducing the predicted value below the current experimental bounds [25, 50]. One could then investigate whether these finely tuned parameter points allow for a strong EWPT. However, this approach relies on substantial cancellations that are highly sensitive to the choice of renormalization scheme for the fermion masses (e.g., $\overline{\text{MS}}$ vs. on-shell) [25], and are generally expected to be unstable under higher-order corrections. Consequently, this strategy introduces significant theoretical uncertainty, rendering such parameter points unreliable for drawing firm conclusions about the viability of EWBG in the C2HDM.

We here follow a different approach. Rather than imposing the experimental limits as a strict constraint on the parameter space, we indicate the predicted values across our benchmark planes. This facilitates a direct and quantitative comparison between theoretical predictions and experimental bounds, making it possible to assess the level of tension in regions relevant for successful EWBG. There are compelling reasons to quantify this tension, rather than eliminate all C2HDM parameter points which do not satisfy the limit on the electron EDM. In the C2HDM, the electron EDM and the BAU both arise from the same unique source of CP violation. This tight connection enhances predictability but also means that EDM constraints strongly impact the viability of the C2HDM as a framework for EWBG. However, this tight correlation can be relaxed in more general frameworks.

For example, introducing a hard breaking of the \mathbb{Z}_2 symmetry imposed in the C2HDM allows for additional CP-violating phases in the Higgs potential and the Yukawa sector. Regarding the latter, a possibility to have CP-violating phases while suppressing flavour-changing neutral currents consists of the so-called flavour alignment [91, 92]. Such models can suppress the predicted electron EDM while maintaining the CP violation required for EWBG [18, 93–95]. It is important to note, however, that this approach comes with several caveats: (1) a significant fine-tuning is required between different and, a-priori, unrelated sources of CP violation to suppress the EDMs, (2) the suppression is generally only possible for one specific fermion EDM, leaving other EDMs unsuppressed, (3) the hard \mathbb{Z}_2 -breaking in the Higgs sector induces flavor-changing neutral currents that are tightly constrained, and (4) the flavor alignment is not stable under the running group evolution, introducing further naturalness issues.

Alternative but theoretically more elegant approaches involve the introduction of additional fields. For instance, the addition of gauge-singlet scalars or further scalar doublets forming a dark/hidden sector can lead to the so-

called *secluded* CP violation, where CP-violating interactions are confined to couplings involving dark-sector particles [40, 96–98]. Then, EDMs are generated only at higher loop orders beyond the two-loop level relevant in the C2HDM. This setup can suppress EDMs to acceptable levels, but it typically involves more parameters, less predictivity, and potentially additional constraints from dark matter phenomenology. Another elegant idea is the so-called *transient* CP violation, where new CP-violating sources are active only during the high-temperature epoch of the early universe and vanish at zero temperature [41, 99, 100]. This naturally suppresses EDMs today but requires more complex models to dynamically realise a period of transient CP violation in the early universe.

Lastly, some proposals [68, 101, 102] aim to suppress the electron Yukawa coupling, thereby reducing the leading contributions to the electron EDM, which then arise only at higher loop orders. While this can potentially bring the EDM prediction below current experimental limits, such suppression is typically ad hoc and challenging to realise within a UV-complete framework [103]. Moreover, this approach does not address EDM contributions for other fermions or composite particles (such as neutrons or molecules), which remain sensitive to CP-violating effects and may yield constraints.

D. Thermal history and description of the EWPT

To study the dynamics of the EWPT in the C2HDM, we employ the public code `BSMPT v.3` [54–56], which computes the one-loop daisy-resummed finite-temperature effective potential in the Landau gauge and using an on-shell-like renormalization scheme. In this approach, the total effective potential is given by

$$V(\Phi_i, T) = V_{\text{tree}}(\Phi_i) + V_{\text{CW}}(\Phi_i) + V_{\text{CT}}(\Phi_i) + V_{\text{T}}(\Phi_i, T) + V_{\text{daisy}}(\Phi_i, T). \quad (16)$$

V_{tree} is the tree-level potential shown in Eq. (3), V_{CW} consists of zero-temperature radiative corrections in the form of the usual Coleman-Weinberg potential renormalized in the $\overline{\text{MS}}$ scheme [104]. V_{CT} contains UV-finite counterterm contributions that are defined in such a way as to cancel the first and second derivatives of V_{CW} with respect to the fields in the tree-level EW minimum. This enforces on-shell-like renormalization conditions at zero temperature in order to maintain the tree-level values of the vacuum expectation values and the scalar masses at one-loop level [11]. This prescription also facilitates the decoupling of radiative corrections for heavy particles [105].⁵ Finally, thermal corrections that explicitly depend on the temperature T are contained in V_{T} and

⁵It should be noted that the true pole masses of the scalars also receive momentum-dependent corrections which are neglected if the

V_{daisy} [106], which include the one-loop thermal corrections and corrections from the resummation of daisy diagrams, respectively, following the Arnold-Espinosa prescription [107].

BSMPT traces the temperature-dependent vacuum structure by numerically identifying all phases, taking into account all four possible field directions in terms of the vevs shown in Eq. (7). If a pair of co-existing vacua in a certain temperature range is detected, a first-order phase transition from the false vacuum $\phi_{i,\text{false}}$ into the true vacuum $\phi_{i,\text{true}}$ is possible, where ϕ_i in the discussion of this section collectively denotes the scalar background fields. The critical temperature T_c is defined as the temperature at which the vacua are degenerate. The actual phase transition occurs at the lower nucleation temperature T_n , where bubbles of the true-vacuum phase can nucleate and expand.⁶

The decay rate per unit volume as a function of the temperature is given by [108, 109]

$$\Gamma(T) = A(T)e^{-S_3(T)/T}, \quad (17)$$

where $S_3(T)$ is the three-dimensional Euclidean action of the bounce solution describing the bubble, and $A(T)$ is a prefactor with mass dimension four. The condition for the onset of the phase transition is that on average one bubble nucleates per Hubble volume, which for EWPTs (approximating the sub-leading prefactor as $A(T) = T^4$) corresponds to [110]

$$\frac{S_3(T_n)}{T_n} \approx 140. \quad (18)$$

This condition defines the nucleation temperature T_n . The bounce action S_3 is computed by finding the O(3)-symmetric bounce solution $\phi_{i,b}(\rho)$ that extremises the Euclidean action

$$S_3(T) = 4\pi \int_0^\infty d\rho \rho^2 \left[\frac{1}{2} \left(\frac{d\phi_i}{d\rho} \right)^2 + V(\phi_i, T) \right], \quad (19)$$

where ρ is the radial coordinate of the bubble. Determining $\phi_{i,b}(\rho)$ amounts to solving the equation of motion (or bounce equations)

$$\frac{d^2\phi_i}{d\rho^2} + \frac{2}{\rho} \frac{d\phi_i}{d\rho} = \nabla V(\phi_i), \quad (20)$$

subject to the boundary conditions

$$\phi_i(\rho \rightarrow \infty) = \phi_{i,\text{false}}, \quad \left. \frac{d\phi_i}{d\rho} \right|_{\rho=0} = 0. \quad (21)$$

finite counterterm shifts are derived from the effective potential. While the momentum-dependent corrections are neglected in this approach, numerically they are expected to be small.

⁶The differences between nucleation, percolation and completion temperatures are small for EWPTs in the C2HDM, where the possible amount of supercooling is very limited. We therefore focus on the nucleation temperature in our discussion for simplicity.

The code BSMPT solves this set of differential equations using the path deformation algorithm [111].

The EWPT can be characterized by four key thermal parameters: the strength of the transition α , the inverse duration in Hubble units β/H , the nucleation temperature T_n , and the bubble wall velocity v_w [112]. The parameter α can be defined in terms of the trace of the energy-momentum tensor,

$$\alpha = \frac{1}{\rho_R} \left[\Delta V(T) - \frac{T}{4} \frac{\partial \Delta V(T)}{\partial T} \right]_{T_n}. \quad (22)$$

Here, $\Delta V(T) = V_{\text{false}} - V_{\text{true}}$ with $V_{\text{false}} = V(\phi_{i,\text{false}})$ and $V_{\text{true}} = V(\phi_{i,\text{true}})$ is the difference in the effective potential between the false and true vacua, and $\rho_R = \pi g_{\text{eff}} T^4/30$ is the background energy density assuming a radiation dominated universe, with g_{eff} being the effective degrees of freedom. Larger values of α correspond to stronger phase transitions. The inverse duration β/H can be calculated with

$$\frac{\beta}{H} = T_n \frac{\partial}{\partial T} \left(\frac{S(T)}{T} \right) \Big|_{T_n}, \quad (23)$$

where H is the Hubble parameter.

Finally, the bubble wall velocity v_w is an important parameter influencing the dynamics of the phase transition, the resulting BAU, and the peak frequency and amplitude of the resulting GW spectrum. However, unlike the parameters α and β/H , it is difficult to compute reliably as it requires solving out-of-equilibrium transport equations that account for the friction between the moving wall and the surrounding plasma. We estimate the bubble wall velocity following the simplified toy model presented in Ref. [10]. In particular, we use the relation between v_w and the strength parameter α derived in that work for the C2HDM in order to assign a value of v_w to each parameter point featuring an EWPT. Typical values for the wall velocity in our setup fall within the range $0.1 \lesssim v_w \lesssim 0.25$. This interval agrees fairly well with the values for v_w that were found for a selection of parameter points the inert 2HDM in Ref. [113].

1. Electroweak baryogenesis

The baryon asymmetry can be dynamically generated during a strong first-order EWPT via EWBG [4]. An essential condition for successful EWBG is a sufficiently strong EWPT. This is typically quantified in terms of the baryon number preservation criterion (or baryon washout condition) [4, 37]

$$\xi_n \equiv \frac{v_n}{T_n} \gtrsim 1, \quad (24)$$

where, in the C2HDM, the EW symmetry breaking vev in the true minimum at the nucleation temperature T_n

is given by

$$v_n = v(T_n) = \sqrt{v_1^2(T_n) + v_2^2(T_n) + v_{\text{CP}}^2(T_n)}. \quad (25)$$

The washout condition ensures that baryon-number violating sphaleron processes are suppressed in the broken phase and that the generated BAU is preserved after the transition completes.⁷

Instead of solving the full set of transport equations to compute the BAU in the C2HDM, we make use of the results from Refs. [7, 10, 116] in which the transport equations were studied with the CP-violating source term computed in the WKB approximation [117, 118] and focusing on the top-quark transport which is the relevant contribution in the C2HDM. To estimate the baryon asymmetry generated during the EWPT, we adopt the analytic approximation introduced in Ref. [41]. In this framework, the baryon-to-entropy ratio is given by

$$\frac{\eta_s}{10^{-11}} \approx 6 \cdot 10^2 \frac{\sin(\delta_t) \xi_n^2}{L_W T_n}, \quad (26)$$

where L_W is the thickness of the bubble wall and T_n is the nucleation temperature.⁸ The phase δ_t encodes the CP-violating source relevant for baryogenesis, and depends on t_β through the top-quark Yukawa coupling,

$$\delta_t = \frac{\Delta\theta}{1 + t_\beta^2}, \quad (27)$$

with $\Delta\theta$ denoting the variation of the CP-violating phase of the top Yukawa across the bubble wall [7]

$$\Delta\theta = \theta_{\text{true}} - \theta_{\text{false}}. \quad (28)$$

Working in the basis in which the CP-violating vev is contained in Φ_2 , see Eq. (7), the CP phase in the true minimum can be computed with the vevs in the global minimum, such that

$$\theta_{\text{true}} = \tan^{-1} \left(\frac{v_{\text{CP,true}}}{v_{2,\text{true}}} \right). \quad (29)$$

For the CP phase in the false minimum, this formula cannot be applied because in the C2HDM we find (in most cases) $v_{2,\text{false}} = 0$. Instead, we compute θ_{false} using the field profile of the bounce solution $\phi_i(\rho)$, see the discussion in Section IID, in the limit $\rho \rightarrow \infty$, i.e [41]

$$\lim_{\rho \rightarrow \infty} = \tan^{-1} \left(\frac{\phi_{\text{CP}}(\rho)}{\phi_2(\rho)} \right), \quad (30)$$

⁷The baryon number preservation criterion defined in this way is known to exhibit a residual gauge dependence [114]. In this work, we evaluate the criterion using the effective potential in Landau gauge, where the impact of this dependence is expected to be subdominant compared to other sources of theory uncertainty [115], such as renormalization scale dependence, missing higher-order corrections, and ambiguities in the thermal resummation procedure [20].

⁸ η_s is related to η_γ , see Eq. (1), via the relation $\eta_s \approx \eta_\gamma/7.04$.

where the field profiles $\phi_{\text{CP}}(\rho)$ and $\phi_2(\rho)$ were obtained by solving the bounce equations as discussed in Section IID. Finally, we compute L_w following Ref. [10] by fitting the field profile of $v_2(\rho)$ with a kink profile of the form

$$\phi_2(\rho) = \frac{\phi_2(0) - \phi_2(\infty)}{2} \left(1 - \tanh \frac{\rho}{L_w} \right) + \phi_2(\infty). \quad (31)$$

Since the true bubble profile is only approximated by the kink profile, as a cross check, we fitted also $\phi_1(\rho)$ with the same kink profile to verify if the results for L_w are consistent. The values for L_w obtained with either $\phi_2(\rho)$ or $\phi_1(\rho)$ were in good agreement.

The results of Refs. [10, 116], and consequently also the estimate of the baryon-to-entropy ratio η_s shown in Eq. (26), rely on the gradient expansion, whose validity breaks down for too thin bubbles with $L_w T_n \lesssim 2$. We find for the EWPT in our benchmark planes values of $L_w T_n > 2$, see the discussion in Appendix B, such that the gradient expansion is applicable. Nevertheless, we stress that the approximation applied here provides only a qualitative estimate of the BAU, enabling us to identify regions of parameter space that are favoured by a successful realisation of EWBG. Should future LHC data provide indications favouring a specific realisation of the C2HDM that allows a sufficiently strong EWPT, it would be well motivated to pursue a more refined and quantitatively more robust computation of the baryon asymmetry within that particular scenario.

An additional source of uncertainty on the prediction for the BAU arises from its dependence on the bubble wall velocity v_w . For large wall velocities $v_w \approx 1$, the generated asymmetry is known to be significantly suppressed (see Ref. [119] for a recent discussion). In our analysis, we estimate the baryon asymmetry using an approximation valid in the regime of slow-moving (subsonic) bubble walls where there is only a minor dependence on v_w [7, 10]. Using the method discussed in Section IID, the predicted bubble wall velocities remain below $v_w \approx 0.3$, well within the range where the approximation remains reliable and only mildly depends on v_w . Therefore, we do not consider an additional suppression from fast-moving bubble walls.

2. Gravitational wave relics

First-order cosmological phase transitions generate a stochastic background of GWs [120, 121], potentially observable by future space-based GW interferometers. In the case of an EWPT, the resulting GW spectrum typically peaks in the millihertz range, precisely where detectors like LISA are most sensitive [122, 123].

In the 2HDM, the dominant contributions to the GW signal arise not from the bubble wall collisions themselves, but from the bulk motion of the thermal plasma induced by expanding bubbles. These include long-lasting sound waves and magnetohydrodynamic turbu-

lence [10]. To model the resulting GW spectrum, we use numerical power-law fits derived from hydrodynamical simulations, expressing the spectral shape, amplitude, and peak frequency as functions of the four key phase transition parameters discussed in Section II D. The specific formulas for the spectral shape of the total GW signal $h^2\Omega_{\text{GW}}$ are taken from Ref. [22], which uses the results presented in Refs. [110, 124]. We consider the contributions from sound waves and turbulence,

$$h^2\Omega_{\text{GW}} = h^2\Omega_{\text{sw}} + h^2\Omega_{\text{turb}}, \quad (32)$$

where the dominant contribution is $h^2\Omega_{\text{sw}}$.

The detectability of a stochastic GW signal is determined by the signal-to-noise ratio (SNR) given by

$$\text{SNR} = \sqrt{\mathcal{T} \int_{-\infty}^{+\infty} df \left[\frac{h^2\Omega_{\text{GW}}(f)}{h^2\Omega_{\text{Sens}}(f)} \right]^2}, \quad (33)$$

where \mathcal{T} is the exposure time, and $h^2\Omega_{\text{Sens}}$ denotes the nominal detector sensitivity to stochastic sources [125]. In our analysis, we focus on LISA and assume a nominal mission duration of $\mathcal{T} = 7$ years. A stochastic GW typically is considered to be detectable if the SNR is larger than one. However, taking into account the substantial theoretical uncertainties in the predictions for the GW signals [32–34], we consider a GW signal to be potentially detectable with LISA if the SNR exceeds the threshold $\text{SNR} > 10^{-3}$, as further discussed below.

III. RESULTS

In this section, we present our numerical results for the benchmark planes that we define in the C2HDM. We explore parameter space regions where a strong first-order EWPT is realised. Among these, we indicate where the BAU can be explained via EWBG, and we indicate where the GW signal is predicted to be sufficiently strong to be potentially detectable with LISA.

For each parameter point that yields a first-order EWPT with $\xi_n > 0.8$, the corresponding value of ξ_n is represented by the colour of the point. We choose a threshold value of 0.8, which is slightly smaller than the value 1 appearing in the baryon number preservation criterion shown in Eq. (24), since the predictions for ξ_n are subject to sizable theoretical uncertainties. In particular, while we employ the Arnold-Espinosa resummation prescription, it was shown recently for the real 2HDM in Ref. [20] that a more consistent thermal resummation via partial dressing predicts smaller nucleation temperatures, and therefore larger values of ξ_n compared to the Arnold-Espinosa prescription.

Similarly, the predictions for the baryon-to-entropy ratio η_s are subject to large uncertainties, not only from those related to the parameters characterising the EWPT, such as the bubble wall velocity [119], but also from uncertainties associated with the derivation

of the CP-violating source terms in the transport equations [126]. Taking this into account, the blue lines in our plots indicate the parameter ranges that predict strong first order EWPT and values of η_s in the range of range $\eta_s^{\text{exp}}/2 \leq \eta_s \leq 2\eta_s^{\text{exp}}$, with $\eta_s^{\text{exp}} \approx 8.7 \cdot 10^{-11}$, which should be seen as as regions indicating a successful of the EWBG.

Regarding GWs, we adopt a threshold of $\text{SNR} > 10^{-3}$ for identifying potentially detectable GW signals with LISA, rather than the commonly used threshold of $\text{SNR} > 1$. This choice is motivated by significant theoretical uncertainties in the prediction of the GW spectrum. For instance, our computation of the bubble wall velocity v_w yields subsonic values $v_w \lesssim 0.2$ for the bulk of parameter points, based on the approach detailed in Section II D. However, the dominant sound wave contribution to the GW signal peaks for larger velocities, $v_w \approx c_s \approx 0.6$, where c_s is the speed of sound in the relativistic plasma. If the true bubble wall velocity is underestimated in our setup, the predicted SNRs could be smaller by one to two orders of magnitude compared to scenarios where $v_w \approx c_s$ is assumed [22].⁹ Moreover, recent work [20] in the R2HDM using a more refined thermal resummation scheme called partial dressing [128] has found stronger EWPTs than those predicted with the Arnold-Espinosa method employed here. Although the parameter regions favourable for an EWPT remain unchanged, the nucleation temperatures using the partial dressing approach were found to be lower by a factor of two in the considered benchmark point. This would enhance the GW signal by roughly two orders of magnitude. In light of these considerations we use a lower SNR threshold to identify scenarios that may yield observable signals at LISA once theoretical uncertainties are better understood.¹⁰

1. Smoking gun scenario

The first benchmark plane that we define is motivated by results obtained in the CP-conserving R2HDM. In the R2HDM, the strongest EWPT were found for scenarios featuring the alignment limit $\cos(\beta - \alpha) \approx 0$ and a sizable mass gap with $m_A > m_H$, with $m_{H\pm} \approx m_A$, and $M \approx m_H$ to satisfy theoretical and experimental constraints, see the discussion above. We construct our C2HDM benchmark plane by fixing the scalar masses based on these R2HDM results, and we study the impact

⁹Recent numerical real-time simulations of the bubble growth beyond the local thermal equilibrium approximation show detonation with $v_w \approx 1$ instead of deflagration solution $v_w \lesssim c_s$ under certain conditions [127].

¹⁰The detectability of a predicted GW signal ultimately depends on additional theoretical uncertainties from the hydrodynamics of GW production and experimental uncertainties such as unknown astrophysical or cosmological foregrounds. These considerations lie beyond the scope of this work.

of CP violation in the C2HDM by varying the mixing angles α_1 and α_3 . Specifically, we vary α_1 in a range around the alignment condition, $\sin(\beta - \alpha_1) \approx 0$. The other mixing angle α_3 used as input parameter is varied around $\alpha_3 \approx 0$. Then, the lighter BSM neutral scalar h_2 remains predominantly CP-even (corresponding to the state H in the R2HDM limit), while the heavier neutral BSM scalar h_3 remains predominantly CP-odd (corresponding to the state A in the CP-conserving R2HDM).

Concretely, the benchmark plane smoking gun (**BP-SG**) is defined by

$$\begin{aligned} \textbf{BP-SG: } & -0.3 \leq s_{\beta-\alpha_1} \leq 0.3, \quad -0.2 \leq \alpha_3 \leq 0.2, \\ & t_\beta = 3, \quad m_{h_2} = M = 420 \text{ GeV}, \\ & m_{h_3} = m_{H^\pm} = 660 \text{ GeV}. \end{aligned} \quad (34)$$

The size of the splitting between m_{h_2} and m_{h_3} is chosen to be in the interval where we found a strong EWPT in the R2HDM in Ref. [23], associated with a GW signal potentially in reach of LISA. The value of $t_\beta = 3$ is sufficiently large to avoid the current cross-section limits from the smoking gun signature $h_3 \rightarrow Zh_2$ with $h_2 \rightarrow t\bar{t}$ performed by ATLAS and CMS [129, 130], but small enough to not suppress significantly the predicted BAU, which approximately scales with a factor of $1/t_\beta^2$ as shown in Eq. (27).

The results for the benchmark plane **BP-SG** are shown in Fig. 1a. We find an area featuring a strong EWPT for values of $-0.10 \lesssim s_{\beta-\alpha_1} \lesssim 0.16$ and $|\alpha_3| \lesssim 0.25$. Close to the CP-conserving limit $\alpha_3 \approx 0$, this region only spans to smaller values of $s_{\beta-\alpha_1} \approx 0.11$ because there the one-loop potential becomes unbounded and the EW vacuum at zero temperature is unstable.¹¹ Larger values of ξ_n correspond to stronger EWPTs. Within the region of parameter space predicting a first-order EWPT, the values of ξ_n (defined in Eq. (24) and indicated by the colour scale) tend to increase as $|s_{\beta-\alpha_1}|$ and α_3 decrease, reaching their maximum near the alignment limit where the Higgs boson h_1 has SM-like couplings. This can be understood intuitively by the fact that the scalars involved as dynamical fields in the EWPT should be as light as possible in order to increase the strength of the phase transition [12], just as in the SM, where the strengths decrease with increasing Higgs boson mass (with all other parameters fixed) [5]. In the alignment limit, the mass eigenstate basis is identical to the Higgs basis [47], in which only the lightest scalar h_1 obtains a vev during EW symmetry breaking. However, for $\beta \neq \alpha_1$ and/or $\alpha_3 \neq 0$, also the field directions corresponding to the heavier states h_2 and/or h_3 would obtain a vev, respectively, which weakens the strength of the EWPT.

In the area of points with an EWPT, we find a nested region in the interval $-0.10 \lesssim s_{\beta-\alpha_1} \lesssim -0.03$ where no EWPT is predicted, and accordingly no points are displayed. In this nested area the condition shown in Eq. (18) for the on-set of the phase transition is never met due to a too large potential barrier separating the true and false minima, and the universe remains trapped in the unphysical vacuum with unbroken EW symmetry although a deeper EW-symmetry breaking minimum exists at $T = 0$. This *vacuum trapping* effect has been studied in detail in the R2HDM in Ref. [22], highlighting that it excludes parameter space regions in which otherwise the potentially strongest EWPTs would be found, thus diminishing the prospects for the detection of GWs at LISA. We observe here in the C2HDM that for all values of $s_{\beta-\alpha_1}$ and $\alpha_3 \approx 0$ where the vacuum trapping forbids the presence of an EWPT, there is a non-vanishing value of α_3 where the EWPT takes place. This indicates that the C2HDM is able to mitigate the impact of vacuum trapping observed in the R2HDM by introducing small CP-violating mixings via $\alpha_3 \neq 0$.

Substantial parts of the parameter region predicting a strong EWPT are already excluded by LHC constraints, whose exclusions are indicated with the grey shaded area. Only the area within the black solid lines passes the limits from all BSM scalar searches included in HiggsTools. The parameter regions to the left and to the right of the allowed area are excluded by CMS searches for the resonant pair production of the 125 GeV Higgs boson via the decay $h_2 \rightarrow h_1 h_1$, based on a CMS combination of searches in $b\bar{b}b\bar{b}$, $b\bar{b}\tau^+\tau^-$, $b\bar{b}\gamma\gamma$ and $b\bar{b}W^+W^-$ final states [131]. The regions above and below the allowed region are excluded by searches for $h_2 \rightarrow Zh_1$ with subsequent decay $h_1 \rightarrow b\bar{b}$, performed by ATLAS [71]. Within the allowed region, the currently most sensitive LHC searches are the ones for the smoking gun signature $h_3 \rightarrow Zh_2$ with the lighter BSM state h_2 decaying into $t\bar{t}$ pairs [129, 130], for which the cross sections remain sizable in and around the alignment limit because only BSM scalars are involved. The fact that searches for multi-Higgs signatures (where either the SM-like Higgs or another scalar is produced in the decay of a heavier BSM spin-0 resonance) already exclude significant portions of the otherwise viable parameter space, or constitute the most sensitive probes of the remaining regions, highlights their increasing relevance for testing the electroweak phase transition in future LHC runs. We also find them in this benchmark plane to be significantly more constraining than the limits from the cross-section measurements of the 125 GeV Higgs boson, which also become relevant away from the alignment limit.

Within the region consistent with current LHC constraints, we find that successful EWBG can be achieved, as indicated by the blue solid line that encloses the parameter points predicting $\eta_s^{\text{exp}}/2 \leq \eta_s \leq 2\eta_s^{\text{exp}}$. To the right and bottom of this blue region, the observed BAU cannot be reproduced because the EWPT becomes too weak, leading to smaller values of ξ_n , which enters

¹¹The impact of vacuum instabilities would be more severe considering only the tree-level potential, excluding parameter points with an EWPT for values of $s_{\beta-\alpha_1} \gtrsim 0.025$ at $\alpha_3 \approx 0$ and values of $s_{\beta-\alpha_1} \gtrsim 0.090$ at $\alpha_3 \approx \pm 0.25$ (see the discussion in Section II C 1).

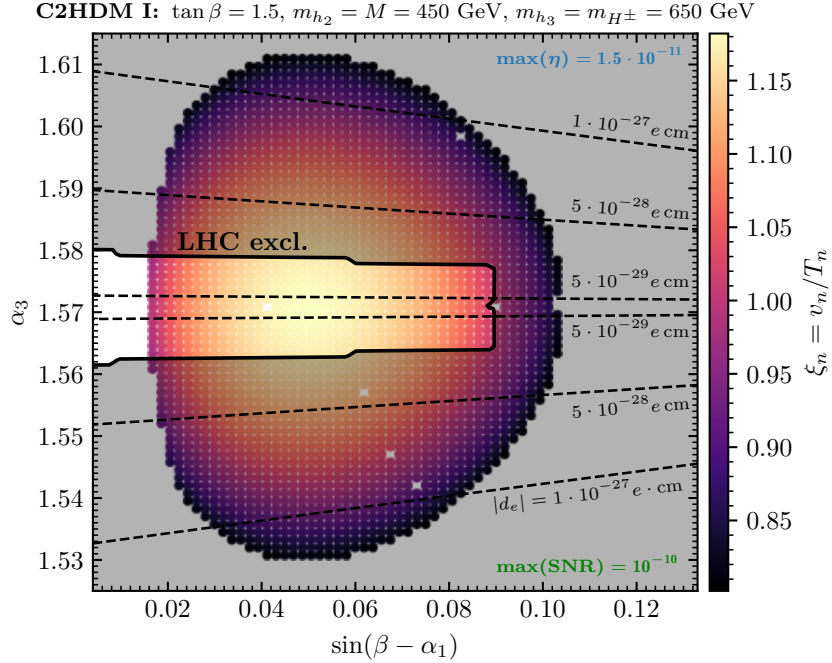
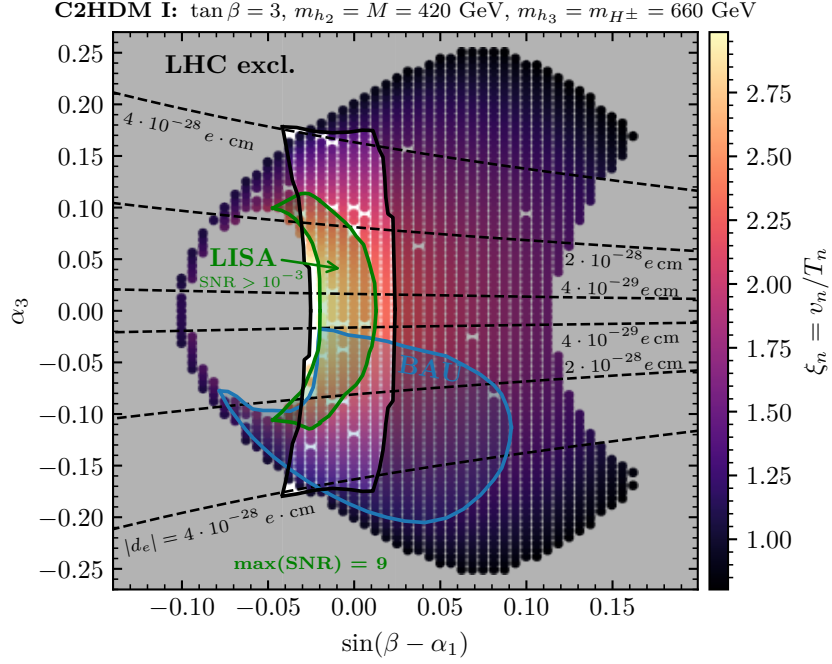


FIG. 1. Shown are parameter points in the $\{\sin(\beta - \alpha_1), \alpha_3\}$ planes that predict a strong first-order EWPT, with the color of each point indicating the corresponding value of ξ_n . The remaining C2HDM parameters are fixed as specified in the plot headers. The grey shaded areas are excluded by cross section limits from BSM scalar searches at the LHC. The green area indicates parameter space regions featuring a GW signal with a LISA SNR larger than $\text{SNR} > 10^{-3}$ assuming an exposure time of 7 years. Taking into account the sizable theoretical uncertainties, these areas can potentially be probed with LISA (see the text for details). The blue area indicates parameter regions with the baryon-to-entropy ratio η_s predicted to be in the range $\eta_s^{\text{exp}}/2 \leq \eta_s \leq 2\eta_s^{\text{exp}}$. Finally, the dashed black lines are contour lines indicating the prediction for the electron EDM $|d_e|$. In the lower plot no green and blue regions are visible because the EWPT is not sufficiently strong to give rise to a detectable GW signal or to a baryon-to-entropy ratio in agreement with observations, respectively.

quadratically in the numerator of Eq. (26), and larger values of $L_w T_n$ in the denominator. To the left of the blue region, vacuum trapping prevents the transition from completing, therefore precluding electroweak baryogenesis. Finally, in the parameter region on top of the blue region, where $|\alpha_3|$ is very small, the amount of CP violation (contained in the parameter δ_t in Eq. (26)) is not sufficient to facilitate EWBG.

The parameter region suitable for EWBG is associated with detectable values of the electron EDM, indicated in Fig. 1a with the black dashed contour lines. We find that in the blue region the electron EDM values exceed $|d_e| = 4 \cdot 10^{-29} e \cdot \text{cm}$, in tension with the currently strongest experimental bound of $|d_e| < 4.1 \times 10^{-30} e \cdot \text{cm}$ [39] by about an order of magnitude or more. Hence, in the absence of cancellation mechanisms beyond the C2HDM, the electron EDM constraint excludes the parameter region favourable for EWBG in the **BP-SG** plane. Alternatively, new sources of CP violation can be considered that facilitate EWBG without inducing values of $|d_e|$ above the experimental limits, in which case in this plane the parameter space region with vanishing α_3 would become suitable for EWBG. (see the discussion in Section II C 5 for more details).

We also indicate in Fig. 1a with the green solid line the parameter space regions in which the EWPT is sufficiently strong to produce a primordial GW background that would potentially be detectable at LISA, with a $\text{SNR} > 10^{-3}$ as discussed above. The SNRs of the predicted GW signals peak around the alignment limit, with a maximum value of $\text{SNR}_{\text{max}} \approx 9$. We find an overlap between the blue region and the green region that is compatible with the current LHC constraints from BSM scalar searches and the cross section measurements of the 125 GeV Higgs boson. This demonstrates that although the presence of CP violation required for EWBG reduces the strength of the EWPT in this scenario, the EWPT is still strong enough to produce a potentially detectable GW signal. We note here that using a stronger requirement of $\text{SNR} > 1$ would not change this conclusion. However, the overlap between the green and the blue areas would shrink substantially. The overlapping blue and green region is already partially ruled out by LHC searches for resonant Higgs boson pair production, see the discussion above. Moreover, it is expected to be within reach of upcoming LHC Run 3 searches for the smoking gun process $h_3 \rightarrow h_2 Z \rightarrow (t\bar{t})Z$ [23, 36]. These searches can be evaded if the value of t_β is increased, but this would also lower the predicted BAU. In Section III 3 we discuss the t_β -dependence of the predicted BAU in more detail.

2. Inverted smoking gun scenario

Now we turn to the analysis of a scenario that we refer to as the benchmark plane with an inverted smoking gun signal (**BP-ISG**). In contrast to the typical smoking

gun scenario discussed above, we consider mixing angles such that the heaviest neutral scalar is dominantly CP-even, while the lighter BSM neutral scalar is mainly CP-odd, effectively inverting the would-be CP assignments compared to the case in **BP-SG**. This configuration was found to be less prone to realise a strong EWPT in the CP-conserving R2HDM [35]. The main difficulty arises because, for the same value of t_β , the mass gap between the two BSM scalars h_2 and h_3 cannot be made as large without violating theoretical constraints from perturbative unitarity, a problem that becomes increasingly severe the larger t_β . Moreover, another complication observed in the R2HDM is that away from the alignment limit, in **BP-ISG** the heaviest state h_3 acquires a vev, which tends to induce a greater suppression on the strength of the EWPT compared to the typical smoking gun setup **BP-SG**, where the second-lightest state h_2 obtains a vev. In this study, we investigate whether the inverted smoking gun scenario can still support a sufficiently strong EWPT to account for the observed BAU and/or produce GW signals detectable by LISA. As before, we also analyse the impact of CP violation on the strength of the EWPT, going beyond previous studies in the R2HDM.

In Fig. 1b, we show the results of a benchmark scenario of the inverted smoking gun, defined by the parameter plane

$$\begin{aligned} \text{BP-ISG: } & 0 \leq s_{\beta-\alpha_1} \leq 0.15, \\ & \pi/2 - 0.05 \leq \alpha_3 \leq \pi/2 + 0.05, \\ & t_\beta = 1.5, \quad m_{h_2} = M = 450 \text{ GeV}, \\ & m_{h_3} = m_{H^\pm} = 650 \text{ GeV}. \end{aligned} \quad (35)$$

Due to the values of $\alpha \approx \pi/2$, the CP assignments of the neutral BSM Higgs bosons are flipped compared to the scenario discussed in Section III 1: here h_2 is predominantly CP-odd and lighter, while h_3 is heavier and mostly CP-even. As a result, the process $h_3 \rightarrow h_2 Z$ resembles the decay $H \rightarrow A Z$ in the CP-conserving limit.

As seen in Fig. 1b, the strongest first-order EWPTs occur in the vicinity of $\alpha_3 \approx \pi/2$, where the CP mixing is minimal, and the mass eigenstates approximately align with the CP eigenstates. Comparing Fig. 1b with Fig. 1a, one can observe that the interval of $1.53 \lesssim \alpha_3 \lesssim 1.61$ that can predict a strong EWPT is significantly smaller than the α_3 -range compatible with a strong EWPT in the smoking-gun scenario. This indicates that the inverted smoking-gun scenario shows less compatibility between the presence of an EWPT and CP-violation in the Higgs potential.

Overall, the strongest EWPTs are centered around the alignment limit $s_{\beta-\alpha_1} \approx 0$ and $\alpha_3 \approx \pi/2$, occurring at slightly positive values of $s_{\beta-\alpha_1}$. However, this shift away from $s_{\beta-\alpha_1} = 0$ is so small that the modifications of the couplings of the 125 GeV Higgs are well in agreement with LHC cross section measurements [132, 133]. For instance, modifications of the coupling of h_1 to massive gauge bosons remain below 1%, and the couplings of h_1 to fermions shows modifications of at most 5% in the

parameter space region not excluded by LHC searches for additional Higgs bosons (see the discussion below). We thus conclude that the **BP-ISG** supports the general expectation in the C2HDM that a strong EWPT is associated with a 125 GeV Higgs boson whose properties, within current LHC experimental precision, remain indistinguishable from those of a SM Higgs boson.

The values of ξ_n that we find in this benchmark plane are at most reaching $\xi_n \approx 1.2$, thus barely satisfying the condition shown in Eq. (24) that prevents the washout of the BAU after the transition, and which is required for a realisation of EWBG. As a consequence of the smaller strengths of the EWPTs and the smaller amount of CP-violation due to the more restricted range for α_3 , no region in the benchmark plane reaches a BAU sufficient to match the observed baryon-to-entropy ratio, as indicated by the absence of blue contours in Fig. 1b. Additionally, there is no green area because the GW signals are predicted to be much weaker across the parameter space, with a maximum LISA SNR of $\text{SNR} \approx 10^{-10}$, far below the sensitivity threshold of LISA. This is consistent with the relatively weak strength of the phase transition, as encoded in the moderate values of $\xi_n \approx 1$.

In principle, the prospects for a strong EWPT in this inverted smoking-gun scenario could be improved by increasing the mass splitting between h_2 and h_3 , which tends to enhance the strength of the transition. This can be achieved by simultaneously choosing smaller values of t_β , thereby avoiding a strongly coupled regime and maintaining agreement with perturbative unitarity. However, reducing t_β also intensifies the tension with current LHC searches, while the absence of signals for BSM Higgs bosons already imposes stringent constraints on this region of parameter space.

The parameter regions that are excluded by the current cross section limits from LHC searches are shaded in grey, and only the small region within the solid black line is still allowed. The shape of the allowed parameter region in this scenario is largely dictated by an ATLAS combination of searches targeting the resonant pair production of the 125 GeV Higgs boson in the $b\bar{b}b\bar{b}$, $b\bar{b}\tau^+\tau^-$, and $b\bar{b}\gamma\gamma$ final states [74], which exclude the areas above and below the allowed band. In addition, ATLAS searches for spin-0 resonances decaying into a Z boson and a 125 GeV Higgs boson [71] exclude points with a strong EWPT located to the right of this region. A key difference compared to the previously discussed benchmark plane in Section III 1 lies in the nature of the decaying state h_2 . In the inverted smoking-gun scenario **BP-ISG** discussed here, the relevant decay is $h_2 \rightarrow h_1 h_1$, where h_2 is predominantly CP-odd. This decay is forbidden in the CP-conserving limit (i.e. for $\alpha_3 = \pi/2$), but becomes allowed when $\alpha_3 \neq \pi/2$, thereby shaping the upper and lower bounds of the viable parameter space in Fig. 1b. In contrast, in the benchmark scenario **BP-SG** discussed in Section III 1, h_2 was mainly CP-even, and its decay to a pair of 125 GeV Higgs bosons is suppressed near the alignment limit but becomes possible for $s_{\beta-\alpha_1} \neq 0$, re-

gardless of whether CP is conserved. In that case, the resonant di-Higgs searches primarily excluded parameter points on the left and right edges of the allowed region.

As in the smoking gun scenario **BP-SG** discussed above, in the still allowed parameter regions in the inverted smoking gun scenario **BP-ISG**, the current most sensitive LHC search is the smoking gun searches for $h_3 \rightarrow h_2 Z$ with $h_2 \rightarrow t\bar{t}$. In these searches, the experimental strategies carried out by ATLAS [129] and CMS [130] do not allow for a distinction between the CP properties of the Higgs bosons involved. Therefore, in the CP-conserving limit, a potential observation in this channel could originate from either $A \rightarrow ZH$ or $H \rightarrow ZA$ decays, assuming both processes correspond to the same total cross section. Recently, a proposal has been put forward to gain sensitivity to the CP nature of the Higgs bosons by exploiting angular observables sensitive to the spin correlations of the $t\bar{t}$ system produced in the decay of the lighter Higgs boson [36]. Our results strengthen the case for the scenario where the heavier resonance is mainly CP-odd and the lighter is mainly CP-even, as it could explain the matter-antimatter asymmetry and predict detectable GW signals, whereas the scenario with the inverted CP assignments **BP-ISG** is not able to. Hence, being able to experimentally distinguish between the two in the most sensitive channel is of key relevance to understand the physics underlying EW symmetry breaking.

The parameter plane **BP-ISG** with inverted smoking gun remains viable due to a slight excess in the ATLAS data from $h_3 \rightarrow Zh_2$ searches around masses of 450 GeV and 650 GeV for the two spin-0 resonances, which weakens the cross section limits [129]. However, the predicted cross sections are approximately equal to the 95% confidence level limits recently reported by CMS [130], which are still not finally published and therefore not yet included in **HiggsTools**. Moreover, the direct production of h_2 decaying via $h_2 \rightarrow t\bar{t}$ contributes to $t\bar{t}$ and $t\bar{t}t\bar{t}$ final states. The investigated benchmark plane is compatible with the first-year Run 2 results from CMS $t\bar{t}$ searches [81], but the CP-conserving limit $\alpha_3 \approx \pi/2$ would be in tension with the full Run 2 ATLAS [134] and CMS results [135]. However, these updated limits are not included here since they can only be applied under the assumption of CP conservation where h_2 and h_3 do not interfere. As shown in Ref. [82], interference effects between the two scalars can be significant in the presence of CP violation and must be properly taken into account. Also there are significant uncertainties in modeling the SM $t\bar{t}$ background near the di-top threshold. In particular, CMS presented limits both with and without a toponium bound state contribution, leading to fundamentally different exclusions. Additionally, the ATLAS and CMS results show substantial discrepancies that remain unresolved. Theoretically more robust limits are available from searches in the $t\bar{t}t\bar{t}$ final state using the full Run 2 data carried out by both ATLAS [84] and CMS [83], excluding values of $t_\beta \lesssim 1.2$ for a pseudoscalar Higgs boson at a mass of about 450 GeV. A similar lower limit is ob-

tained from searches for the charged scalars H^\pm via the decay $H^\pm \rightarrow tb$ [136]. Considering that the benchmark plane **BP-ISG** barely escapes the limits from several different LHC searches, we expect that the inverted smoking gun scenarios will be almost fully probed by Run 3 LHC searches. The only way to avoid these searches would be to increase t_β , while at the same time we would have to decrease the mass splitting between h_2 and h_3 to satisfy perturbative unitarity constraints. However, this would further suppress the strength of the EWPTs and the amount of the predicted BAU, which in the studied benchmark plane is already below the observed value.

To summarise, although the inverted scenario **BP-ISG** still supports a strong EWPT but it is much less favourable for EWBG and does not predict detectable GW signals. The combination of weaker phase transitions, suppressed BAU generation, and tighter LHC (and EDM constraints) suggests that achieving viable EWBG in this regime would require new dynamics to enhance the strength of the EWPT and/or additional CP-violating sources not contained in the (\mathbb{Z}_2 symmetric) C2HDM.

3. Aligned smoking gun scenario

In this section, we investigate a third benchmark plane, which we refer to as the aligned smoking gun scenario **BP-ASG**. Unlike the previous two benchmark planes, where the mixing angle α_1 was varied, here we fix α_1 by imposing the alignment condition $s_{\beta-\alpha_1} = 0$, which ensures SM-like couplings of the 125 GeV Higgs boson in the CP-conserving limit $\alpha_3 \approx 0$. We maintain a sizable mass gap between the two heavier neutral scalars h_2 and h_3 to facilitate a strong EWPT, as it was the case in the original smoking gun scenario **BP-SG** discussed in Section III 1. Instead of varying α_1 , we explore different values of t_β , motivated by the interplay between collider constraints and EWBG. While small t_β is favoured for successful EWBG due to enhanced top-quark transport, it also leads to larger production cross sections of the BSM scalars at the LHC. To study the impact of CP violation in this context, we additionally vary the CP-violating angle α_3 , as in the two benchmark planes discussed above.

We define the benchmark plane **BP-ASG** as

$$\begin{aligned} \textbf{BP-ASG: } & 1.5 \leq t_\beta \leq 20, \quad -0.3 \leq \alpha_3 \leq 0.0, \\ & s_{\beta-\alpha_1} = 0, \quad m_{h_2} = M = 420 \text{ GeV}, \\ & m_{h_3} = m_{H^\pm} = 660 \text{ GeV}. \end{aligned} \quad (36)$$

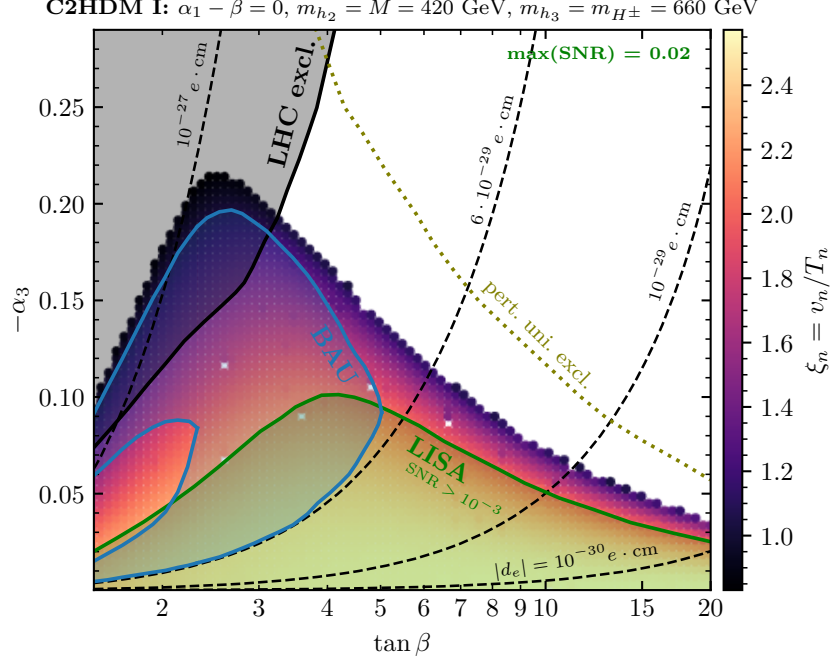
The results for this benchmark plane are shown in Fig. 2a. As in the original smoking gun scenario **BP-SG** discussed in Section III 1, the strongest EWPTs are found in the CP-conserving alignment limit, i.e. at $\alpha_3 = 0$, across the entire t_β range. In this limit, the strength of the EWPT is independent of t_β due to the condition $m_{h_2} = M$. For fixed t_β , increasing $|\alpha_3|$ leads to a gradual weakening of the phase transition, in line with

the behaviour observed in the benchmark plane **BP-SG**, see Fig. 1a. We find that for $t_\beta \approx 2.5$ the presence of a strong EWPT is compatible with the largest amount of CP violation in the Higgs sector: strong transitions are still possible for values of $|\alpha_3| \approx 0.2$ (with $\alpha_3 < 0$ to ensure the correct sign of the BAU). For smaller $t_\beta \approx 1.5$, the possible range shrinks to roughly $|\alpha_3| < 0.1$, and for values of $t_\beta \approx 20$ it is further reduced to approximately $|\alpha_3| \lesssim 0.03$. All points predicting a strong EWPT in this benchmark plane are found to be consistent with theoretical constraints from tree-level perturbative unitarity, which excludes only the upper right corner as indicated with the dotted olive line.

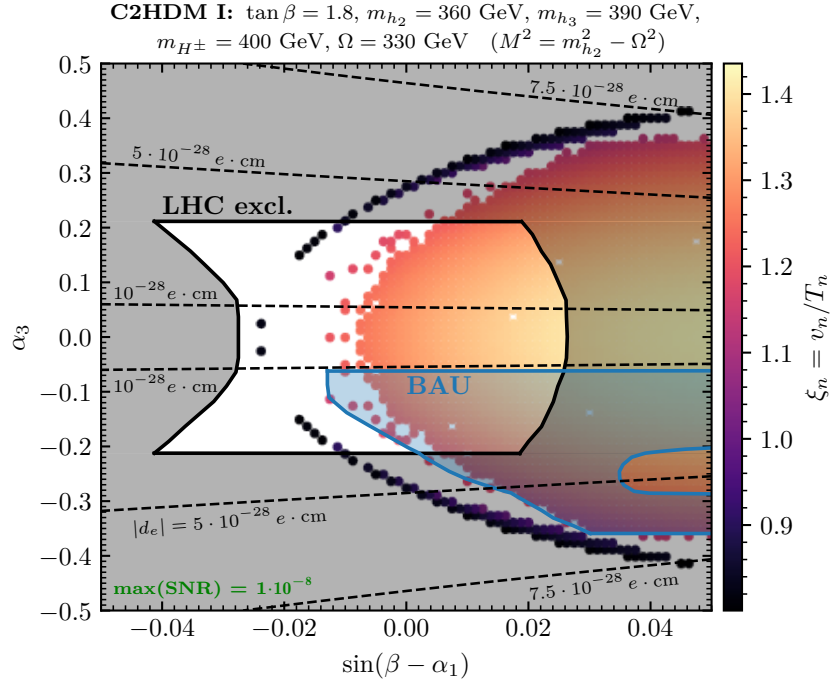
The blue shaded region in Fig. 2a indicates the parameter space where the predicted BAU lies within a factor of two of the observed value, which we take as the acceptable range given theoretical uncertainties; see the discussion in Section IID 1. One can see that successful EWBG is possible for t_β values roughly up to values of $t_\beta \approx 5$. At low $t_\beta \lesssim 2.3$, there is a hole in the blue region where the predicted BAU exceeds the upper bound of our assumed uncertainty band, i.e. it is more than twice the observed value. For larger values of $t_\beta \gtrsim 5$, on the other hand, the top transport becomes too suppressed to generate the observed asymmetry, and the predicted BAU falls below the acceptable range. The presence of this upper limit on t_β for successful EWBG defines a clear target region for LHC searches probing the extended Higgs sector of the C2HDM, as will be discussed in detail below.

As with other benchmarks, the electron EDM poses a strong constraint. The dashed black contours indicate values exceeding $|d_e| = 6 \cdot 10^{-29} e \cdot \text{cm}$ throughout the parameter region suitable for EWBG. This again implies that, in the absence of either a cancellations or other suppression mechanisms, the C2HDM parameter space region compatible with EWBG would be ruled out by the recent experimental upper limits on the electron EDM.

The prospects for detecting a GW signal at LISA are illustrated by the green-shaded region in Fig. 2a, which corresponds to parameter points where the EWPT generates a GW signal with a SNR above 0.001. As discussed in Section III, this threshold is chosen to account for the significant theoretical uncertainties that affect GW predictions from cosmological phase transitions [32]. The green region spans the entire t_β -range shown in the plot. As expected, the largest SNRs occur in the CP-conserving limit at $\alpha_3 \approx 0$, corresponding to the alignment limit, $s_{\beta-\alpha_1} = 0$, where the EWPTs are the strongest. For non-zero values of α_3 , the detectable GW region extends at most up to $|\alpha_3| \approx 0.1$ at $t_\beta \approx 4$. For $t_\beta \lesssim 5$, there is an overlap between the blue (BAU-favoured) and green (GW-detectable) regions, indicating that in this part of parameter space the EWPT could simultaneously account for the observed BAU and produce a GW signal potentially within reach of LISA. As discussed further below, this overlapping region is also expected to be testable at the LHC via searches for additional Higgs bosons, offering a compelling interplay be-



(a) **BP-ASG:** aligned smoking-gun scenario for a strong first-order EWPT with a mass gap between a lighter and mainly CP-even state h_2 and a heavier mainly CP-odd state h_3 .



(b) **BP-AMD:** scenario with almost mass degenerate BSM states and a strong first-order EWPT

FIG. 2. Shown are parameter points with a strong first-order EWPT in a $\{t_\beta, \alpha_3\}$ plane in the upper plot and a $\{s_{\beta-\alpha_1}, \alpha_3\}$ plane in the lower plot. The colour coding of the points and the grey, blue and green regions are defined as in Fig. 1. In the lower plot no green region is visible because the EWPT is not sufficiently strong to give rise to a detectable GW signal.

tween the LHC and LISA in probing the nature of the EWPT and EWBG. However, this region is in significant tension with the most recent experimental upper limits on the electron EDM, as discussed above, which should be taken into account when interpreting these results.

For larger t_β -values, the green region extends beyond the blue one, especially for small CP-violating phases with $\alpha_3 \approx 0$, reflecting the fact that the strongest transitions occur in the CP-conserving limit, where the phase transition dynamics are largely independent of t_β . Consequently, GW signals can remain detectable even when the BAU cannot be generated. In the context of the type I Yukawa structure considered here, probing these large t_β -scenarios at the LHC becomes increasingly challenging because one approaches the so-called fermiophobic limit, where the main production cross sections of the BSM Higgs bosons are strongly suppressed. In contrast, other Yukawa types feature enhanced couplings to bottom quarks and/or tau leptons at large t_β , potentially allowing the LHC to probe this parameter space region via the decays of the heavy Higgs bosons into $b\bar{b}$ and $\tau^+\tau^-$ final states. Therefore, especially in the C2HDM type I, it is well possible that a GW signal compatible with an EWPT in the C2HDM could be detected by LISA without any possibility for a complementary discovery of a BSM Higgs boson at the LHC. The only collider trace of the EWPT would then be an enhanced self coupling of the 125 GeV Higgs boson that might be accessible at the high-luminosity phase of the LHC, see the discussion in Section II C 4.

We close the discussion of the benchmark plane **BP-ASG** by addressing the key question of how well the BAU-favoured region can be tested at the LHC, both now and in future runs. The currently excluded parameter space is indicated by the grey shaded region in the upper left corner of the plot, which overlaps with the region favoured for EWBG at $t_\beta \lesssim 3$ and $|\alpha_3| \gtrsim 0.06$. This exclusion originates from ATLAS searches for the decay of the state h_2 into a Z boson and a 125 GeV Higgs boson [71]. These searches lose sensitivity at smaller values of $|\alpha_3|$, since the tree-level coupling $h_2 h_1 Z$ vanishes in the alignment limit, and they become less effective at larger t_β due to the approximate $1/t_\beta^2$ suppression of the gluon-fusion production cross section of h_2 . In most parts of the remaining viable region that accounts for the BAU, the currently most sensitive probe is the smoking gun signature $h_3 \rightarrow h_2 Z$, with h_2 decaying into a top-quark pair [129, 130], in agreement with the results in the smoking-gun scenario **BP-SG** discussed in Section III 1.

Looking ahead, a central question is whether the LHC will be able to fully cover the C2HDM parameter space that can realise EWBG, which we here find to span up to values of $t_\beta \approx 5$. Based on the projections from Ref. [88], searches in the four-top final state are expected to significantly improve sensitivity to the state h_2 at 420 GeV. While current limits from these searches exclude values of $t_\beta \lesssim 1$ for a dominantly CP-even h_2 , the projected improvement of cross section limits by a factor

of about 4-5 at the high-luminosity LHC would extend coverage up to $\tan\beta \approx 2-3$. Similar reach in t_β can be expected from searches in the di-top final state, though their sensitivity depends more strongly on the CP nature of h_2 [82]. Searches for the charged Higgs bosons may also be relevant in this regime, currently excluding in this scenario parameter space with $t_\beta \lesssim 1.2$ for a mass of about 660 GeV [136], although the lack of official projections prevents a definitive assessment. For $t_\beta \lesssim 3$, all these channels could compete in sensitivity with the smoking gun process. At higher t_β , however, the smoking gun channel becomes increasingly dominant, as the slight increase of the branching ratio for $h_3 \rightarrow h_2 Z$ partially compensates the $1/t_\beta^2$ drop in h_3 production. To estimate the future reach of the smoking gun search, we rescale the Run 2 ATLAS limits [129] using the expected increase in statistics by a factor of $\sqrt{3000 \text{ fb}^{-1}/140 \text{ fb}^{-1}}$, corresponding to the expected integrated luminosity at the end of the high-luminosity LHC. This extrapolation suggests that the BAU region could be probed up to $\tan\beta \approx 4$. When taking into account the slightly higher center-of-mass energy at the high-luminosity LHC and potential systematic improvements (see also Ref. [36]), it appears realistic that the smoking gun searches may ultimately probe the entire C2HDM parameter space suitable for EWBG in benchmark scenarios in which the presence of the EWPT relies on the hierarchical spectrum with a lighter dominantly CP-even BSM Higgs boson and a heavier dominantly CP-odd BSM Higgs boson.

4. Almost mass-degenerate scenario

The fourth and final benchmark plane we define represents a qualitatively different scenario from those analysed previously. The benchmark planes **BP-SG**, **BP-ISG** and **BP-ASG** relied on a sizable mass splitting between the additional neutral Higgs bosons to induce a strong first-order EWPT. In contrast, this scenario features an approximately degenerate spectrum for the neutral and charged BSM scalars. In this setup, the potential barrier between the EW symmetric and broken phases required for a strong EWPT stems from sizable quartic couplings that arise due to a separation between the physical scalar masses and the soft \mathbb{Z}_2 -breaking scale M defined in Eq. (11). This mechanism is motivated by the detailed study in Ref. [12], where the relevant conditions for realising a strong EWPT in the 2HDM with a degenerate scalar spectrum were systematically explored and contrasted with the case of hierarchical mass spectra. Additional support for this setup comes from Ref. [14], where explicit C2HDM benchmark points with approximately degenerate BSM scalars were found that featured a strong EWPT and satisfied Run 1 LHC and electron EDM constraints available at the time.

Specifically, we consider a benchmark plane denoted as the almost mass-degenerate (**BP-AMD**) scenario de-

finied by

$$\begin{aligned}
\textbf{BP-AMD: } & -0.05 \leq s_{\beta-\alpha_1} \leq 0.05, \quad -0.5 \leq \alpha_3 \leq 0.5, \\
& t_\beta = 1.8, \quad m_{h_2} = 360 \text{ GeV}, \\
& m_{h_3} = 390 \text{ GeV}, \quad m_{H^\pm} = 400 \text{ GeV}, \\
& \Omega = m_{h_2}^2 - M^2 = 330 \text{ GeV}^2, \quad (37)
\end{aligned}$$

where the parameter Ω was defined in Ref. [10] to parametrise the splitting between the scale M and the almost degenerate Higgs bosons masses m_{h_2} , m_{h_3} and m_{H^\pm} .

The parameter values defining this benchmark plane are carefully chosen to optimise the conditions for a strong EWPT within a degenerate scalar spectrum while remaining consistent with theoretical and LHC constraints. As in the previously discussed benchmark planes **BP-SG** and **BP-ISG**, we vary the mixing angles α_1 and α_3 , where α_1 is scanned around the alignment limit condition $s_{\beta-\alpha_1} = 0$. The scan range for α_3 is taken to be substantially broader than in the previous benchmark planes. This is possible because, in the present scenario, and in contrast to hierarchical mass spectra, the near-degeneracy of the neutral scalars h_2 and h_3 allows for sizable CP admixtures without violating theoretical constraints. The value of $t_\beta = 1.8$ is chosen to be as small as feasible, since lower values generally enhance the prospects for a strong EWPT by allowing larger values of the splitting parameter Ω without conflicting with perturbative unitarity constraints [12]. However, values of t_β much below the chosen value are ruled out by LHC searches for additional Higgs bosons, in particular from searches for the charged scalars [136]. The BSM Higgs bosons are required to remain relatively light in this scenario to ensure sufficiently large non-decoupling effects which are essential for generating a strong EWPT while not being in tension with perturbative unitarity and vacuum stability constraints [12]. Consequently, all BSM Higgs masses are chosen just above the di-top threshold, where viable parameter space remains because LHC searches in the $\tau^+\tau^-$ [137, 138], W^+W^- [139, 140] and ZZ [141, 142] final states start to lose sensitivity in type I. Finally, after fixing the angles and masses, the splitting parameter Ω is set to a value inspired by the analysis in Ref. [12], such that a strong EWPT is obtained in the alignment limit. At the same time, the value of Ω is kept moderate enough to avoid generating quartic scalar couplings in conflict with perturbative unitarity bounds or vacuum stability constraints.

The results for the benchmark plane **BP-AMD** are shown in Fig. 2b. Despite the absence of large mass hierarchies, which facilitates the strongest EWPTs, this scenario can still realise a strong first-order EWPT. As before, the colour coding of the points in the $\{s_{\beta-\alpha_1}, \alpha_3\}$ plane indicates the strength of the phase transition through the value of ξ_n . We observe that the strongest transitions $\xi_n \approx 1.4$ are reached in the CP-conserving limit for low values of $\alpha_3 \approx 0$. The values of ξ_n that can be achieved here are significantly smaller than the max-

imum values of $\xi_n \approx 3$ that we found in scenarios with a hierarchical spectrum, see the scenario **BP-SG** shown in Fig. 1a, but they satisfy the baryon-number preservation condition shown in Eq. (24). This demonstrates that the EWPTs predicted in an almost mass degenerate scenario might be sufficiently strong for a realising EW baryogenesis.

The blue contour marks the region where the predicted baryon-to-entropy ratio η_s is compatible with the observed value within an uncertainty of a factor of two. This viable BAU region arises despite the near-degeneracy of the scalar states, suggesting that successful EWBG does not strictly require a large mass gap between the neutral BSM Higgs bosons in the C2HDM. Accordingly, the smoking gun signature $h_3 \rightarrow Zh_3$ is not distinctive of this scenario (see also the discussion in Refs. [14]). However, as we will discuss in detail below, other LHC searches can probe and likely exclude (or confirm) this benchmark plane in the near future.

The parameter space region viable for EWBG is again in tension with the most recent constraints on the electron EDM. The dashed black lines show constant contours $|d_e|$, which exceed $|d_e| \approx 10^{-28} e \cdot \text{cm}$ in the blue region preferred by EWBG, well above the experimental bound of $|d_e| < 4.1 \cdot 10^{-30} e \cdot \text{cm}$. The tension with the non-observation of an electron EDM in this scenario is about a factor of two more severe compared to the scenarios **BP-SG** and **BP-ASG**. This increased tension can be attributed to the overall lighter BSM Higgs boson spectrum in agreement with expectation following Eq. (13). Moreover, in comparison to **BP-SG**, the smaller value of t_β leads to larger predictions for the electron EDMs.

The limited strength of the EWPTs places the predicted GW signals below the sensitivity of the LISA experiment. The predicted GW signal is extremely suppressed. The maximum SNR in LISA for this benchmark is $\text{SNR}_{\text{max}} \approx 10^{-8}$, which is much below the sensitivity threshold of LISA and is effectively unobservable in future space-based GW interferometers. This aligns with expectations that compressed spectra tend to yield weaker transitions, smaller latent heat and lower bubble wall velocities, reducing the efficiency of GW production. This implies that any hints that might be revealed in future LHC searches consistent with this scenario would point to an EWPT without a corresponding stochastic GW background detectable at LISA.

The LHC constraints on this benchmark plane are illustrated by the grey-shaded exclusion regions and the solid black contour enclosing the remaining viable parameter space. The excluded regions to the left and right of the allowed area arise from searches for the state h_2 , targeting the decay $h_2 \rightarrow ZZ$ [142], which become increasingly sensitive as one departs from the alignment condition $s_{\beta-\alpha_1} = 0$. At the mass of $h_2 = 360 \text{ GeV}$ considered here, we find these searches to be more constraining than the searches for resonant Higgs boson pair production via $h_2 \rightarrow h_1 h_1$ decays. The parameter space regions above and below the allowed region are excluded by searches

targeting the $h_2 \rightarrow h_1 Z$ decay mode [71]. In this benchmark plane, these searches begin to be the most sensitive search channel for h_2 at values of $|\alpha_3| \gtrsim 0.05$. One can see that the two searches responsible for the shape of the exclusion region already exclude a substantial part of the blue region that is favoured by EWBG.

The parameter choices in the benchmark plane **BP-AMD** were deliberately optimized to evade existing LHC bounds, but the remaining viable region is expected to be comprehensively tested as the LHC collects more data. Several search channels, while not currently excluding this scenario, lie just below the sensitivity threshold and will soon become decisive. In particular, searches for the charged Higgs bosons through the $H^\pm \rightarrow tb$ decay already constrain slightly smaller values of t_β , and for the chosen value of $t_\beta = 1.8$ the predicted cross sections are only about 10% below the current 95% confidence level limits [136]. As a result, charged Higgs boson searches are likely to probe this almost mass degenerate C2HDM scenario even at moderately larger t_β (or m_{H^\pm}), though EWBG restricts t_β from becoming too large. Moreover, very close to and within the alignment limit, the channels $h_{2,3} \rightarrow t\bar{t}$ [81], $h_2 \rightarrow \tau^+\tau^-$ [138, 143] and $h_3 \rightarrow \gamma\gamma$ [144] become the most sensitive probes, filling in the gaps left by the searches in the ZZ and $h_1 Z$ final states responsible for the exclusion contours, which lose sensitivity in this region. These channels offer the exciting prospect of observing not only a single additional Higgs boson, but potentially the entire extended scalar sector predicted in such a scenario. Additional coverage outside of the alignment limit is also expected from searches for resonant pair production of the SM-like Higgs boson via $h_2/h_3 \rightarrow h_1 h_1$ decays [73, 74]. Altogether, the current configuration of this benchmark represents a carefully chosen and narrow window that has thus far escaped exclusion from LHC searches. However, with ongoing and future LHC runs it appears likely that the remaining gaps will be closed, potentially already with the data collected during Run 3, making the benchmark **BP-AMD** a fully testable realisation of EWBG.

In summary, **BP-AMD** highlights that viable EWBG remains possible even in the absence of large scalar mass splitting, though such scenarios face major challenges from stringent LHC constraints that will soon confirm or exclude if such a C2HDM scenario is realised in nature. The fact that the LHC can probe these scenario is crucial since the predicted GW signals are significantly below the expected sensitivity of future space-based GW experiments, which therefore will not be able to probe such a scenario.

IV. SUMMARY AND CONCLUSIONS

In this work, we have presented an analysis of the EWPT and the possibility to explain the imbalance between matter and antimatter within the C2HDM, a 2HDM with softly broken \mathbb{Z}_2 symmetry and explicit CP

violation in the Higgs potential. The C2HDM is the simplest scalar extension of the SM that features new sources of CP violation and can accommodate a strong first-order EWPT, both vital ingredients for a explaining the matter-antimatter asymmetry through EWBG. Rather than performing fully general parameter scans, we have focused on defining well-motivated benchmark planes, which enables a more transparent analysis of how CP violation influences the dynamics of the EWPT in the C2HDM compared to the extensively studied (CP-conserving) R2HDM. This also allows for a more illustrative analysis of the impact of the key LHC search channels that can probe the still allowed parameter space regions relevant for successful EWBG. The benchmark planes are intended to guide ongoing efforts in defining representative scenarios for the exploration of CP-violation in extended scalar sectors at the LHC Run 3 and beyond, while remaining consistent with current collider constraints and theoretical requirements.

It should be noted that we have not imposed the electron EDM bounds as a hard constraint. Taking into account the recent experimental upper bounds, this would leave barely any room for realising EWBG in the C2HDM. Instead, we evaluated and displayed the predicted electron EDM values across the benchmark planes in order to quantify the degree of tension with the most recent experimental limits. This reflects the possibility that the electron EDM may be suppressed in more general extensions of the C2HDM, without altering the dynamics of the EWPT.

Primordial GW signals offer an additional, complementary probe of the EWPT. We have assessed the potential detectability of a stochastic GW background produced from an EWPT within the C2HDM, using the predicted SNR for the LISA experiment as a reference. Taking into account the sizeable theoretical uncertainties associated with the modelling of the phase transition dynamics and GW production, we used a lower SNR threshold of 0.001 instead of the more conventional value of 1. This choice reflects the challenges in accurately predicting the strength of GW signals from the EWPT, while still allowing us to identify regions of parameter space where detectable signals could potentially be observed by LISA. One of the key questions addressed in our work is whether EWBG and detectable GW signals can be simultaneously realised, and if so, which parameter space regions can accommodate both. Furthermore, we examined the LHC signals that correspond to these regions in order to explore the potential interplay between the LHC and space-based GW astronomy in probing EWBG in the next decade.

In total, we explored four distinct benchmark planes: the smoking gun scenario **BG-SG** shown in Fig. 1a, the inverted smoking gun scenario **BP-ISG** shown in Fig. 1b, the aligned smoking gun scenario **BP-ASG** shown in Fig. 2a, and the almost mass degenerate scenario **BP-AMD** shown in Fig. 2b. The first three benchmark scenarios share the feature that the presence of the strong

EWPT relies on a sizeable mass splitting between the neutral BSM Higgs bosons h_2 and h_3 contained in the C2HDM. In the fourth benchmark scenario all neutral and charged BSM Higgs bosons h_2 , h_3 and H^\pm are chosen to be close in mass, and the EWPT is facilitated by a splitting between the \mathbb{Z}_2 -breaking scale M and the physical masses of the Higgs bosons.

Among the four benchmark planes, all but the inverted smoking gun scenario **BP-ISG** feature parameter regions in which the observed baryon asymmetry can be explained by EWBG. The parameter space regions favoured by EWBG show a tension with the recent experimental upper bounds on the electron EDM by about an order of magnitude or more. This tension is most severe in the almost mass degenerate scenario **BP-AMD** due to an overall lighter Higgs spectrum.

Regarding GWs, only the smoking gun scenario **BP-SG** and the aligned smoking gun scenario **BP-ASG** yield SNRs at LISA of the order of 0.001–10, making them the only scenarios that can potentially be probed with space-based GW experiments. This is consistent with and confirms earlier findings in the R2HDM, where it was shown that a mass hierarchy featuring a lighter BSM CP-even scalar H and a heavier CP-odd scalar A leads to the strongest EWPTs, motivating the designation of the associated $A \rightarrow ZH$ decay channel as a smoking gun signature at the LHC. Within these two benchmark planes, we have found that parts of the region favoured by EWBG and of the region predicting potentially detectable GW signals overlap, promising an interesting interplay between the LHC and LISA in probing EWBG in the C2HDM.

We have shown that, in the presence of CP violation, the strength of the EWPT tends to be reduced compared to the CP-conserving case. Nevertheless, there remains sufficient parameter space with significant amount of CP violation in the Higgs sector that satisfy the baryon number preservation condition and predicts potentially detectable GW signals. Importantly, in the **BP-SG** scenario we have shown that introducing CP-violating mixing (while keeping other parameters fixed) can help avoid vacuum trapping in the EW-symmetric phase, which would otherwise prevent a phase transition from occurring. As a result, the impact of this vacuum trapping effect, which was observed to frequently prevent the potentially strongest transitions in the R2HDM, can be mitigated in the C2HDM.

On the contrary to the two (aligned) smoking gun scenarios **BP-SG** and **BP-ASG**, for the almost mass degenerate scenario **BP-AMD** and the inverted smoking gun scenario **BP-ISG** we have found that the predicted SNRs remain below the nominal sensitivity of LISA by 8 and 10 orders of magnitude, respectively. This is a consequence of the limited strength of the EWPT in these scenarios. Nevertheless, for the almost mass degenerate scenario **BP-AMD**, we have shown that one can accommodate an EWPT that is sufficiently strong to facilitate EWBG, although this possibility is already

under strong pressure from the non-observation of additional Higgs bosons at the LHC. Since the GW signals predicted in this scenario are far from reaching the detectability threshold of LISA, our results emphasize that observable GWs are not a generic prediction of EWBG in the C2HDM. Due to the tiny SNRs of the order of 10^{-8} or below, this conclusion is unlikely to be affected by the large uncertainties related to the description of cosmological phase transitions and the resulting stochastic GW background. In such cases, the role of the LHC in probing the nature of EW symmetry breaking is especially critical.

Across all four benchmark scenarios considered in this work, current LHC searches already constrain significant portions of the parameter space compatible with a strong first-order EWPT. In the smoking gun scenario **BP-SG**, wide regions are excluded already by searches for resonant Higgs boson pair production ($h_2 \rightarrow h_1 h_1$) and the production of a Higgs boson in association with a Z boson ($h_2 \rightarrow Zh_1$), with the smoking gun channel $h_3 \rightarrow h_2 Z$ (with $h_2 \rightarrow t\bar{t}$) remaining the most sensitive probe in the viable region, centered around the alignment limit. A similar pattern holds in the inverted scenario **BP-ISG**, which only narrowly escapes current limits due to a small excess in ATLAS data from the smoking gun searches in the $Zt\bar{t}$ final state. The inverted scenario requires smaller t_β values to facilitate a strong EWPT, rendering it well within reach of several LHC searches, and is likely to be fully tested during Run 3. The aligned smoking gun scenario **BP-ASG** shows that successful EWBG is possible up to $\tan\beta \approx 5$, with the smoking gun and multi-top signatures, in combination with searches for the production of the 125 GeV Higgs boson from heavier spin-0 resonances, again dominating current and projected sensitivity. Meanwhile, the almost mass-degenerate scenario **BP-AMD**, which was carefully tailored to evade current LHC bounds, lies within reach of various LHC searches targeting the decays $h_{2,3} \rightarrow h_1 h_1$, $h_{2,3} \rightarrow ZZ$, $h_{2,3} \rightarrow Zh_1$, $h_{2,3} \rightarrow \tau^+ \tau^-$, $h_{2,3} \rightarrow \gamma\gamma$, and (most notably) $H^\pm \rightarrow tb$.

In all of the four benchmark planes, searches involving multi-Higgs signatures, where a heavy new Higgs boson decays into final states including the SM-like Higgs boson or another lighter BSM Higgs boson, already exclude large portions of the otherwise viable parameter space or represent the most promising discovery channels. This underscores their growing importance for testing the EWPT at current and future LHC runs. Crucially, it is only during Run 2, with the LHC operating for the first time at 13 TeV center-of-mass energy, that these multi-Higgs and cascade decay signatures have become experimentally accessible, opening uncharted territory in the hunt for additional Higgs bosons. Our results show that the crucial overlap region, where successful EWBG and detectable GW signals coexist, is within the reach of the LHC, particularly through the smoking gun decay channels. This potential interplay between the LHC and LISA strengthens the case for a coordinated effort

to probe the fundamental origin of electroweak symmetry breaking and the BAU. It should be noted, however (as illustrated, e.g. in the aligned smoking gun scenario **BP-ASG**), that the LHC will not be able to cover all parameter regions predicting GW signals detectable at LISA via searches for additional Higgs boson, especially (in type I) at larger t_β . However, larger values of t_β suppress the generation of the BAU. In this case, measurements of the Higgs boson self coupling from non-resonant pair production remain as a final tool to indirectly probe the parameter space during the high-luminosity phase of the LHC.

Altogether, our findings paint a realistic picture of the current status of EWBG in the C2HDM. The parameter space that supports baryogenesis is under increasing pressure from EDM bounds and offers limited prospects for GW detection at LISA. Nonetheless, EWBG in the C2HDM remains phenomenologically interesting, still providing a well-motivated framework for probing the nature of the EWPT during the upcoming LHC Runs. Our benchmark planes are intended to serve as a roadmap for future experimental exploration, while reflecting the evolving experimental constraints that challenge the original motivation for EWBG in the minimal C2HDM. Whether this window can be preserved, or points instead toward extensions beyond the minimal setup, remains an open and timely question.

ACKNOWLEDGMENTS

We thank Howard Haber for useful discussions and Lisa Biermann for helpful correspondence about **BSMPT**. TB acknowledges the support of the Spanish Agencia Estatal de Investigación through the grant “IFT Centro de Excelencia Severo Ochoa CEX2020-001007-S”. The project that gave rise to these results received the support of a fellowship from the “la Caixa” Foundation (ID 100010434). The fellowship code is LCF/BQ/PI24/12040018. MOOR is supported by the STFC under grant ST/X000753/1.

Appendix A: Parameter relations

In order to obtain the Lagrangian parameters from the set of input parameters shown in Eq. (10), we solve numerically for the parameters

$$\alpha_1, \quad \lambda_1, \quad \lambda_2, \quad \lambda_3, \quad \lambda_4, \quad \text{Re } \lambda_5, \quad \text{Im } \lambda_5, \quad (\text{A1})$$

using the following system of equations, where $s_\beta = \sin \beta$, $c_\beta = \cos \beta$ and R_{ij} are the rotation matrix elements defined in Eq. (9),

$$m_{h_1}^2 R_{11}^2 + m_{h_2}^2 R_{21}^2 + m_{h_3}^2 R_{31}^2 = v^2 c_\beta^2 \lambda_1 + m_{12}^2 \tan \beta, \quad (\text{A2})$$

$$m_{h_1}^2 R_{11} R_{12} + m_{h_2}^2 R_{21} R_{22} + m_{h_3}^2 R_{31} R_{32}$$

$$= -m_{12}^2 + v^2 c_\beta s_\beta (\lambda_3 + \lambda_4 + \text{Re } \lambda_5), \quad (\text{A3})$$

$$m_{h_1}^2 R_{11} R_{13} + m_{h_2}^2 R_{21} R_{23} + m_{h_3}^2 R_{31} R_{33} = -\frac{1}{2} v^2 s_\beta \text{Im } \lambda_5, \quad (\text{A4})$$

$$m_{h_1}^2 R_{12}^2 + m_{h_2}^2 R_{22}^2 + m_{h_3}^2 R_{32}^2 = m_{12}^2 \cot \beta + v^2 s_\beta^2 \lambda_2, \quad (\text{A5})$$

$$m_{h_1}^2 R_{12} R_{13} + m_{h_2}^2 R_{22} R_{23} + m_{h_3}^2 R_{32} R_{33} = -\frac{1}{2} v^2 c_\beta \text{Im } \lambda_5, \quad (\text{A6})$$

$$m_{h_1}^2 R_{13}^2 + m_{h_2}^2 R_{23}^2 + m_{h_3}^2 R_{33}^2 = -v^2 \text{Re } \lambda_5 + \frac{m_{12}^2}{s_\beta c_\beta}, \quad (\text{A7})$$

$$m_{H^\pm}^2 = -\frac{1}{2} v^2 (\lambda_4 + \text{Re } \lambda_5) + \frac{m_{12}^2}{s_\beta c_\beta}. \quad (\text{A8})$$

The parameters m_{11}^2 and m_{22}^2 can then be obtained via

$$m_{11}^2 = \frac{m_{12}^2 v_2}{v_1} - \frac{1}{2} v_1^2 \lambda_1 - \frac{1}{2} v_2^2 \lambda_3 - \frac{1}{2} v_2^2 \lambda_4 - \frac{1}{2} v_2^2 \text{Re } \lambda_5, \quad (\text{A9})$$

$$m_{22}^2 = \frac{m_{12}^2 v_1}{v_2} - \frac{1}{2} v_2^2 \lambda_2 - \frac{1}{2} v_1^2 \lambda_3 - \frac{1}{2} v_1^2 \lambda_4 - \frac{1}{2} v_1^2 \text{Re } \lambda_5, \quad (\text{A10})$$

and the imaginary part of m_{12}^2 depends on $\text{Im } \lambda_5$ and is given via Eq. (8). Solving the system of equations given above for $\alpha_3 \neq 0$ leads to two physically distinct solution, from which only one has $\text{Im } \lambda_5 \neq 0$, thus corresponding to a CP-violating parameter point. We always pick this CP-violating solution in our numerical analysis.

Appendix B: Bubble width in the C2HDM

We make use of the results of Refs. [10, 116] to estimate the baryon-to-entropy ratio η_s according to Eq. (26). This approximation for the BAU relies on a gradient expansion of the bubble profile, whose validity breaks down for too thin bubbles with $L_w T_n \lesssim 2$. In order to verify whether the parameter points shown in our benchmark planes satisfy this condition, we show in Fig. 3 the values of $L_w T_n$ that we obtain using the approach discussed in Section IID 1. One can see that the parameter points from the benchmark planes BP-ISG and BP-AMD discussed in Section III 2 and Section III 4, respectively, feature values of $L_w T_n$ that are substantially larger than two. The benchmark planes BP-SG and BP-ASG discussed in Section III 1 and Section III 3, respectively, feature parameter points with stronger EWPT. For the parameter points with the strongest transitions, the values of $L_w T_n$ approach the limit of two, where the application of the gradient expansion becomes problematic. However, this only affects a very small fraction of the parameter points, while the majority of points features values of $L_w T_n \gtrsim 3$. We therefore consider the WKB

framework based on the gradient expansion to be applicable for the bulk of parameter space investigated here.

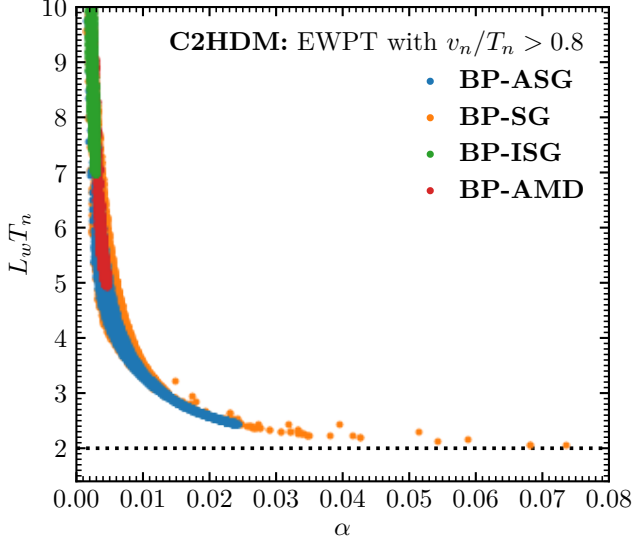


FIG. 3. Predictions for $L_w T_n$ against α for the benchmark planes defined in Section III. BP-ASG: aligned smoking gun scenario (blue), BP-SG: smoking gun scenario (orange), BP-ISG: inverted smoking gun scenario (green), BP-AMD: almost mass degenerate scenario (red). The horizontal dotted line indicates the value $L_w T_n = 2$, where the gradient expansion of the bubble wall profile becomes unreliable.

-
- [1] S. Navas *et al.* (Particle Data Group), *Review of particle physics*, *Phys. Rev. D* **110**, 030001 (2024).
 - [2] A. D. Sakharov, *Violation of CP Invariance, C asymmetry, and baryon asymmetry of the universe*, *Pisma Zh. Eksp. Teor. Fiz.* **5**, 32 (1967).
 - [3] F. R. Klinkhamer and N. S. Manton, *A Saddle Point Solution in the Weinberg-Salam Theory*, *Phys. Rev. D* **30**, 2212 (1984).
 - [4] V. A. Kuzmin, V. A. Rubakov, and M. E. Shaposhnikov, *On the Anomalous Electroweak Baryon Number Nonconservation in the Early Universe*, *Phys. Lett. B* **155**, 36 (1985).
 - [5] K. Kajantie, M. Laine, K. Rummukainen, and M. E. Shaposhnikov, *Is there a hot electroweak phase transition at $m_H \gtrsim m_W$?*, *Phys. Rev. Lett.* **77**, 2887 (1996), [arXiv:hep-ph/9605288](#).
 - [6] M. B. Gavela, P. Hernandez, J. Orloff, and O. Pene, *Standard model CP violation and baryon asymmetry*, *Mod. Phys. Lett. A* **9**, 795 (1994), [arXiv:hep-ph/9312215](#).
 - [7] L. Fromme, S. J. Huber, and M. Seniuch, *Baryogenesis in the two-Higgs doublet model*, *JHEP* **11**, 038, [arXiv:hep-ph/0605242](#).
 - [8] J. M. Cline and P.-A. Lemieux, *Electroweak phase transition in two Higgs doublet models*, *Phys. Rev. D* **55**, 3873 (1997), [arXiv:hep-ph/9609240](#).
 - [9] I. F. Ginzburg, I. P. Ivanov, and K. A. Kanishev, *The Evolution of vacuum states and phase transitions in 2HDM during cooling of Universe*, *Phys. Rev. D* **81**, 085031 (2010), [arXiv:0911.2383 \[hep-ph\]](#).
 - [10] G. C. Dorsch, S. J. Huber, T. Konstandin, and J. M. No, *A Second Higgs Doublet in the Early Universe: Baryogenesis and Gravitational Waves*, *JCAP* **05**, 052, [arXiv:1611.05874 \[hep-ph\]](#).
 - [11] P. Basler, M. Krause, M. Muhlleitner, J. Wittbrodt, and A. Wlotzka, *Strong First Order Electroweak Phase Transition in the CP-Conserving 2HDM Revisited*, *JHEP* **02**, 121, [arXiv:1612.04086 \[hep-ph\]](#).
 - [12] G. C. Dorsch, S. J. Huber, K. Mimasu, and J. M. No, *The Higgs Vacuum Uplifted: Revisiting the Electroweak Phase Transition with a Second Higgs Doublet*, *JHEP* **12**, 086, [arXiv:1705.09186 \[hep-ph\]](#).
 - [13] J. Bernon, L. Bian, and Y. Jiang, *A new insight into the phase transition in the early Universe with two Higgs doublets*, *JHEP* **05**, 151, [arXiv:1712.08430 \[hep-ph\]](#).
 - [14] P. Basler, M. Muhlleitner, and J. Wittbrodt, *The CP-Violating 2HDM in Light of a Strong First Order Electroweak Phase Transition and Implications for Higgs Pair Production*, *JHEP* **03**, 061, [arXiv:1711.04097 \[hep-ph\]](#).
 - [15] W. Su, A. G. Williams, and M. Zhang, *Strong first order electroweak phase transition in 2HDM confronting future Z & Higgs factories*, *JHEP* **04**, 219,

- arXiv:2011.04540 [hep-ph].
- [16] P. Basler, L. Biermann, M. Mühlleitner, and J. Müller, *Electroweak baryogenesis in the CP-violating two-Higgs doublet model*, *Eur. Phys. J. C* **83**, 57 (2023), arXiv:2108.03580 [hep-ph].
 - [17] D. Gonçalves, A. Kaladharan, and Y. Wu, *Electroweak phase transition in the 2HDM: Collider and gravitational wave complementarity*, *Phys. Rev. D* **105**, 095041 (2022), arXiv:2108.05356 [hep-ph].
 - [18] K. Enomoto, S. Kanemura, and Y. Mura, *New benchmark scenarios of electroweak baryogenesis in aligned two Higgs double models*, *JHEP* **09**, 121, arXiv:2207.00060 [hep-ph].
 - [19] D. Gonçalves, A. Kaladharan, and Y. Wu, *Gravitational waves, bubble profile, and baryon asymmetry in the complex 2HDM*, *Phys. Rev. D* **108**, 075010 (2023), arXiv:2307.03224 [hep-ph].
 - [20] P. Bittar, S. Roy, and C. E. M. Wagner, *Self Consistent Thermal Resummation: A Case Study of the Phase Transition in 2HDM*, (2025), arXiv:2504.02024 [hep-ph].
 - [21] M. O. Olea-Romacho, *Primordial magnetogenesis in the two-Higgs-doublet model*, *Phys. Rev. D* **109**, 015023 (2024), arXiv:2310.19948 [hep-ph].
 - [22] T. Biekötter, S. Heinemeyer, J. M. No, M. O. Olea-Romacho, and G. Weiglein, *The trap in the early Universe: impact on the interplay between gravitational waves and LHC physics in the 2HDM*, *JCAP* **03**, 031, arXiv:2208.14466 [hep-ph].
 - [23] T. Biekötter, S. Heinemeyer, J. M. No, K. Radchenko, M. O. Olea-Romacho, and G. Weiglein, *First shot of the smoking gun: probing the electroweak phase transition in the 2HDM with novel searches for $A \rightarrow ZH$ in $\ell^+\ell^-t\bar{t}$ and $\nu b\bar{b}$ final states*, *JHEP* **01**, 107, arXiv:2309.17431 [hep-ph].
 - [24] M. J. Ramsey-Musolf, *The electroweak phase transition: a collider target*, *JHEP* **09**, 179, arXiv:1912.07189 [hep-ph].
 - [25] D. Azevedo, T. Biekötter, and P. M. Ferreira, *2HDM interpretations of the CMS diphoton excess at 95 GeV*, *JHEP* **11**, 017, arXiv:2305.19716 [hep-ph].
 - [26] T. Biekötter, D. Fontes, M. Mühlleitner, J. C. Romão, R. Santos, and J. a. P. Silva, *Impact of new experimental data on the C2HDM: the strong interdependence between LHC Higgs data and the electron EDM*, *JHEP* **05**, 127, arXiv:2403.02425 [hep-ph].
 - [27] S. Weinberg, *Unitarity Constraints on CP Nonconservation in Higgs Exchange*, *Phys. Rev. D* **42**, 860 (1990).
 - [28] I. F. Ginzburg, M. Krawczyk, and P. Osland, in *International Workshop on Linear Colliders (LCWS 2002)* (2002) pp. 703–706, arXiv:hep-ph/0211371.
 - [29] P. Bechtle, O. Brein, S. Heinemeyer, G. Weiglein, and K. E. Williams, *HiggsBounds: Confronting Arbitrary Higgs Sectors with Exclusion Bounds from LEP and the Tevatron*, *Comput. Phys. Commun.* **181**, 138 (2010), arXiv:0811.4169 [hep-ph].
 - [30] H. Bahl, T. Biekötter, S. Heinemeyer, C. Li, S. Paasch, G. Weiglein, and J. Wittbrodt, *HiggsTools: BSM scalar phenomenology with new versions of HiggsBounds and HiggsSignals*, *Comput. Phys. Commun.* **291**, 108803 (2023), arXiv:2210.09332 [hep-ph].
 - [31] T. Biekötter and M. Pierre, *Higgs-boson visible and invisible constraints on hidden sectors*, *Eur. Phys. J. C* **82**, 1026 (2022), arXiv:2208.05505 [hep-ph].
 - [32] D. Croon, O. Gould, P. Schicho, T. V. I. Tenkanen, and G. White, *Theoretical uncertainties for cosmological first-order phase transitions*, *JHEP* **04**, 055, arXiv:2009.10080 [hep-ph].
 - [33] P. Athron, C. Balazs, A. Fowlie, L. Morris, G. White, and Y. Zhang, *How arbitrary are perturbative calculations of the electroweak phase transition?*, *JHEP* **01**, 050, arXiv:2208.01319 [hep-ph].
 - [34] M. Lewicki, M. Merchand, L. Sagunski, P. Schicho, and D. Schmitt, *Impact of theoretical uncertainties on model parameter reconstruction from GW signals sourced by cosmological phase transitions*, *Phys. Rev. D* **110**, 023538 (2024), arXiv:2403.03769 [hep-ph].
 - [35] G. C. Dorsch, S. J. Huber, K. Mimasu, and J. M. No, *Echoes of the Electroweak Phase Transition: Discovering a second Higgs doublet through $A_0 \rightarrow ZH_0$* , *Phys. Rev. Lett.* **113**, 211802 (2014), arXiv:1405.5537 [hep-ph].
 - [36] F. Arco, T. Biekötter, P. Stylianou, and G. Weiglein, *Top-quark spin correlations as a tool to distinguish pseudoscalar $A \rightarrow ZH$ and scalar $H \rightarrow ZA$ signatures in $Zt\bar{t}$ final states at the LHC*, (2025), arXiv:2502.03443 [hep-ph].
 - [37] S. Dimopoulos and L. Susskind, *On the Baryon Number of the Universe*, *Phys. Rev. D* **18**, 4500 (1978).
 - [38] V. Andreev et al. (ACME), *Improved limit on the electric dipole moment of the electron*, *Nature* **562**, 355 (2018).
 - [39] T. S. Roussy et al., *An improved bound on the electron's electric dipole moment*, *Science* **381**, adg4084 (2023), arXiv:2212.11841 [physics.atom-ph].
 - [40] J. M. Cline, K. Kainulainen, and D. Tucker-Smith, *Electroweak baryogenesis from a dark sector*, *Phys. Rev. D* **95**, 115006 (2017), arXiv:1702.08909 [hep-ph].
 - [41] S. J. Huber, K. Mimasu, and J. M. No, *Baryogenesis from transitional CP violation in the early Universe*, *Phys. Rev. D* **107**, 075042 (2023), arXiv:2208.10512 [hep-ph].
 - [42] G. C. Branco, P. M. Ferreira, L. Lavoura, M. N. Rebelo, M. Sher, and J. P. Silva, *Theory and phenomenology of two-Higgs-doublet models*, *Phys. Rept.* **516**, 1 (2012), arXiv:1106.0034 [hep-ph].
 - [43] P. Fayet, *A Gauge Theory of Weak and Electromagnetic Interactions with Spontaneous Parity Breaking*, *Nucl. Phys. B* **78**, 14 (1974).
 - [44] P. Fayet, *Supergauge Invariant Extension of the Higgs Mechanism and a Model for the electron and Its Neutrino*, *Nucl. Phys. B* **90**, 104 (1975).
 - [45] G. Aad et al. (ATLAS), *Observation of a new particle in the search for the Standard Model Higgs boson with the ATLAS detector at the LHC*, *Phys. Lett. B* **716**, 1 (2012), arXiv:1207.7214 [hep-ex].
 - [46] S. Chatrchyan et al. (CMS), *Observation of a New Boson at a Mass of 125 GeV with the CMS Experiment at the LHC*, *Phys. Lett. B* **716**, 30 (2012), arXiv:1207.7235 [hep-ex].
 - [47] J. F. Gunion and H. E. Haber, *The CP conserving two Higgs doublet model: The Approach to the decoupling limit*, *Phys. Rev. D* **67**, 075019 (2003), arXiv:hep-ph/0207010.
 - [48] R. Boto, T. V. Fernandes, H. E. Haber, J. C. Romão, and J. a. P. Silva, *Basis-independent treatment of the complex 2HDM*, *Phys. Rev. D* **101**, 055023 (2020), arXiv:2001.01430 [hep-ph].

- [49] O. M. Ogreid, *Invariants and CP violation in the 2HDM*, PoS **CORFU2017**, 065 (2018), arXiv:1803.09351 [hep-ph].
- [50] D. Fontes, M. Mühlleitner, J. C. Romão, R. Santos, J. a. P. Silva, and J. Wittbrodt, *The C2HDM revisited*, JHEP **02**, 073, arXiv:1711.09419 [hep-ph].
- [51] J. Shu and Y. Zhang, *Impact of a CP Violating Higgs Sector: From LHC to Baryogenesis*, Phys. Rev. Lett. **111**, 091801 (2013), arXiv:1304.0773 [hep-ph].
- [52] S. Inoue, M. J. Ramsey-Musolf, and Y. Zhang, *CP-violating phenomenology of flavor conserving two Higgs doublet models*, Phys. Rev. D **89**, 115023 (2014), arXiv:1403.4257 [hep-ph].
- [53] C.-Y. Chen, S. Dawson, and Y. Zhang, *Complementarity of LHC and EDMs for Exploring Higgs CP Violation*, JHEP **06**, 056, arXiv:1503.01114 [hep-ph].
- [54] P. Basler and M. Mühlleitner, *BSMPT (Beyond the Standard Model Phase Transitions): A tool for the electroweak phase transition in extended Higgs sectors*, Comput. Phys. Commun. **237**, 62 (2019), arXiv:1803.02846 [hep-ph].
- [55] P. Basler, M. Mühlleitner, and J. Müller, *BSMPT v2 a tool for the electroweak phase transition and the baryon asymmetry of the universe in extended Higgs Sectors*, Comput. Phys. Commun. **269**, 108124 (2021), arXiv:2007.01725 [hep-ph].
- [56] P. Basler, L. Biermann, M. Mühlleitner, J. Müller, R. Santos, and J. a. Viana, *BSMPT v3 A Tool for Phase Transitions and Primordial Gravitational Waves in Extended Higgs Sectors*, (2024), arXiv:2404.19037 [hep-ph].
- [57] F. Staub, *Reopen parameter regions in Two-Higgs Doublet Models*, Phys. Lett. B **776**, 407 (2018), arXiv:1705.03677 [hep-ph].
- [58] M. Mühlleitner, M. O. P. Sampaio, R. Santos, and J. Wittbrodt, *ScannerS: parameter scans in extended scalar sectors*, Eur. Phys. J. C **82**, 198 (2022), arXiv:2007.02985 [hep-ph].
- [59] S. Kanemura, T. Kubota, and E. Takasugi, *Lee-Quigg-Thacker bounds for Higgs boson masses in a two doublet model*, Phys. Lett. B **313**, 155 (1993), arXiv:hep-ph/9303263.
- [60] M. E. Peskin and T. Takeuchi, *Estimation of oblique electroweak corrections*, Phys. Rev. D **46**, 381 (1992).
- [61] J. M. Gerard and M. Herquet, *A Twisted custodial symmetry in the two-Higgs-doublet model*, Phys. Rev. Lett. **98**, 251802 (2007), arXiv:hep-ph/0703051.
- [62] F. Mahmoudi, *SuperIso v2.3: A Program for calculating flavor physics observables in Supersymmetry*, Comput. Phys. Commun. **180**, 1579 (2009), arXiv:0808.3144 [hep-ph].
- [63] S. Neshatpour and F. Mahmoudi, *Flavour Physics with SuperIso*, PoS **TOOLS2020**, 036 (2021), arXiv:2105.03428 [hep-ph].
- [64] W. Altmannshofer and P. Stangl, *New physics in rare B decays after Moriond 2021*, Eur. Phys. J. C **81**, 952 (2021), arXiv:2103.13370 [hep-ph].
- [65] A. Tumasyan et al. (CMS), *Measurement of the $B_s^0 \rightarrow \mu^+ \mu^-$ decay properties and search for the $B^0 \rightarrow \mu^+ \mu^-$ decay in proton-proton collisions at $\sqrt{s} = 13$ TeV*, Phys. Lett. B **842**, 137955 (2023), arXiv:2212.10311 [hep-ex].
- [66] R. Aaij et al. (LHCb), *Measurement of the $B_s^0 \rightarrow \mu^+ \mu^-$ decay properties and search for the $B^0 \rightarrow \mu^+ \mu^-$ and $B_s^0 \rightarrow \mu^+ \mu^- \gamma$ decays*, Phys. Rev. D **105**, 012010 (2022), arXiv:2108.09283 [hep-ex].
- [67] M. Misiak and M. Steinhauser, *Weak radiative decays of the B meson and bounds on $M_{H\pm}$ in the Two-Higgs-Doublet Model*, Eur. Phys. J. C **77**, 201 (2017), arXiv:1702.04571 [hep-ph].
- [68] M. Aiko, M. Endo, S. Kanemura, and Y. Mura, *Electroweak baryogenesis in 2HDM without EDM cancellation*, (2025), arXiv:2504.07705 [hep-ph].
- [69] P. Athron, M. J. Ramsey-Musolf, C. Sierra, and Y. Wu, *Electroweak baryogenesis from charged current anomalies in B meson decays*, (2025), arXiv:2502.00445 [hep-ph].
- [70] A. M. Sirunyan et al. (CMS), *Search for a heavy pseudoscalar boson decaying to a Z and a Higgs boson at $\sqrt{s} = 13$ TeV*, Eur. Phys. J. C **79**, 564 (2019), arXiv:1903.00941 [hep-ex].
- [71] G. Aad et al. (ATLAS), *Search for heavy resonances decaying into a Z or W boson and a Higgs boson in final states with leptons and b-jets in 139 fb⁻¹ of pp collisions at $\sqrt{s} = 13$ TeV with the ATLAS detector*, JHEP **06**, 016, arXiv:2207.00230 [hep-ex].
- [72] D. Fontes, J. C. Romão, R. Santos, and J. a. P. Silva, *Undoubtable signs of CP-violation in Higgs boson decays at the LHC run 2*, Phys. Rev. D **92**, 055014 (2015), arXiv:1506.06755 [hep-ph].
- [73] A. M. Sirunyan et al. (CMS), *Combination of searches for Higgs boson pair production in proton-proton collisions at $\sqrt{s} = 13$ TeV*, Phys. Rev. Lett. **122**, 121803 (2019), arXiv:1811.09689 [hep-ex].
- [74] G. Aad et al. (ATLAS), *Combination of Searches for Resonant Higgs Boson Pair Production Using pp Collisions at $\sqrt{s} = 13$ TeV with the ATLAS Detector*, Phys. Rev. Lett. **132**, 231801 (2024), arXiv:2311.15956 [hep-ex].
- [75] A. Tumasyan et al. (CMS), *Search for a heavy Higgs boson decaying into two lighter Higgs bosons in the $\tau\tau b\bar{b}$ final state at 13 TeV*, JHEP **11**, 057, arXiv:2106.10361 [hep-ex].
- [76] G. Aad et al. (ATLAS), *Search for Higgs bosons decaying into new spin-0 or spin-1 particles in four-lepton final states with the ATLAS detector with 139 fb⁻¹ of pp collision data at $\sqrt{s} = 13$ TeV*, JHEP **03**, 041, arXiv:2110.13673 [hep-ex].
- [77] A. Tumasyan et al. (CMS), *Search for a new resonance decaying into two spin-0 bosons in a final state with two photons and two bottom quarks in proton-proton collisions at $\sqrt{s} = 13$ TeV*, JHEP **05**, 316, arXiv:2310.01643 [hep-ex].
- [78] *Search for a new scalar resonance decaying to a Higgs boson and a new scalar with two bottom quarks and two photons in the final state in proton-proton collisions at $\sqrt{s} = 13$ TeV*, Tech. Rep. CMS-PAS-B2G-24-001 (CERN, Geneva, 2025).
- [79] G. Aad et al. (ATLAS), *Search for a resonance decaying into a scalar particle and a Higgs boson in final states with leptons and two photons in proton-proton collisions at $\sqrt{s} = 13$ TeV with the ATLAS detector*, JHEP **10**, 104, arXiv:2405.20926 [hep-ex].
- [80] V. Keus, S. F. King, S. Moretti, and K. Yagyu, *CP Violating Two-Higgs-Doublet Model: Constraints and LHC Predictions*, JHEP **04**, 048, arXiv:1510.04028 [hep-ph].
- [81] A. M. Sirunyan et al. (CMS), *Search for heavy Higgs bosons decaying to a top quark pair in proton-proton*

- collisions at $\sqrt{s} = 13$ TeV, *JHEP* **04**, 171, [Erratum: *JHEP* 03, 187 (2022)], [arXiv:1908.01115 \[hep-ex\]](#).
- [82] H. Bahl, R. Kumar, and G. Weiglein, *Impact of Interference Effects on Higgs-boson Searches in the Di-top Final State at the LHC*, (2025), [arXiv:2503.02705 \[hep-ph\]](#).
- [83] A. M. Sirunyan *et al.* (CMS), *Search for production of four top quarks in final states with same-sign or multiple leptons in proton-proton collisions at $\sqrt{s} = 13$ TeV*, *Eur. Phys. J. C* **80**, 75 (2020), [arXiv:1908.06463 \[hep-ex\]](#).
- [84] G. Aad *et al.* (ATLAS), *Search for $t\bar{t}H/A \rightarrow t\bar{t}t\bar{t}$ production in proton-proton collisions at $\sqrt{s} = 13$ TeV with the ATLAS detector*, (2024), [arXiv:2408.17164 \[hep-ex\]](#).
- [85] S. Kanemura, Y. Okada, and E. Senaha, *Electroweak baryogenesis and quantum corrections to the triple Higgs boson coupling*, *Phys. Lett. B* **606**, 361 (2005), [arXiv:hep-ph/0411354](#).
- [86] G. Aad *et al.* (ATLAS), *Combination of Searches for Higgs Boson Pair Production in pp Collisions at $s=13$ TeV with the ATLAS Detector*, *Phys. Rev. Lett.* **133**, 101801 (2024), [arXiv:2406.09971 \[hep-ex\]](#).
- [87] A. Hayrapetyan *et al.* (CMS), *Constraints on the Higgs boson self-coupling from the combination of single and double Higgs boson production in proton-proton collisions at $s=13$ TeV*, *Phys. Lett. B* **861**, 139210 (2025), [arXiv:2407.13554 \[hep-ex\]](#).
- [88] *Highlights of the HL-LHC physics projections by ATLAS and CMS*, (2025), [arXiv:2504.00672 \[hep-ex\]](#).
- [89] T. Abe, J. Hisano, T. Kitahara, and K. Tobioka, *Gauge invariant Barr-Zee type contributions to fermionic EDMs in the two-Higgs doublet models*, *JHEP* **01**, 106, [Erratum: *JHEP* 04, 161 (2016)], [arXiv:1311.4704 \[hep-ph\]](#).
- [90] D. E. Morrissey and M. J. Ramsey-Musolf, *Electroweak baryogenesis*, *New J. Phys.* **14**, 125003 (2012), [arXiv:1206.2942 \[hep-ph\]](#).
- [91] A. Pich and P. Tuzon, *Yukawa Alignment in the Two-Higgs-Doublet Model*, *Phys. Rev. D* **80**, 091702 (2009), [arXiv:0908.1554 \[hep-ph\]](#).
- [92] M. Jung and A. Pich, *Electric Dipole Moments in Two-Higgs-Doublet Models*, *JHEP* **04**, 076, [arXiv:1308.6283 \[hep-ph\]](#).
- [93] K. Fuyuto, W.-S. Hou, and E. Senaha, *Cancellation mechanism for the electron electric dipole moment connected with the baryon asymmetry of the Universe*, *Phys. Rev. D* **101**, 011901 (2020), [arXiv:1910.12404 \[hep-ph\]](#).
- [94] S. Kanemura, M. Kurota, and K. Yagyu, *Aligned CP-violating Higgs sector canceling the electric dipole moment*, *JHEP* **08**, 026, [arXiv:2004.03943 \[hep-ph\]](#).
- [95] K. Enomoto, S. Kanemura, and Y. Mura, *Electroweak baryogenesis in aligned two Higgs doublet models*, *JHEP* **01**, 104, [arXiv:2111.13079 \[hep-ph\]](#).
- [96] A. Cordero-Cid, J. Hernández-Sánchez, V. Keus, S. F. King, S. Moretti, D. Rojas, and D. Sokolowska, *CP violating scalar Dark Matter*, *JHEP* **12**, 014, [arXiv:1608.01673 \[hep-ph\]](#).
- [97] M. Carena, M. Quirós, and Y. Zhang, *Electroweak Baryogenesis from Dark-Sector CP Violation*, *Phys. Rev. Lett.* **122**, 201802 (2019), [arXiv:1811.09719 \[hep-ph\]](#).
- [98] E. Hall, T. Konstandin, R. McGehee, H. Murayama, and G. Servant, *Baryogenesis From a Dark First-Order Phase Transition*, *JHEP* **04**, 042, [arXiv:1910.08068 \[hep-ph\]](#).
- [99] J. M. Cline and K. Kainulainen, *Electroweak baryogenesis and dark matter from a singlet Higgs*, *JCAP* **01**, 012, [arXiv:1210.4196 \[hep-ph\]](#).
- [100] S. Inoue, G. Ovanessian, and M. J. Ramsey-Musolf, *Two-Step Electroweak Baryogenesis*, *Phys. Rev. D* **93**, 015013 (2016), [arXiv:1508.05404 \[hep-ph\]](#).
- [101] S. Aharony Shapira, *Current bounds on baryogenesis from complex Yukawa couplings of light fermions*, *Phys. Rev. D* **105**, 095037 (2022), [arXiv:2106.05338 \[hep-ph\]](#).
- [102] H. Bahl, E. Fuchs, S. Heinemeyer, J. Katzy, M. Menen, K. Peters, M. Saimpert, and G. Weiglein, *Constraining the CP structure of Higgs-fermion couplings with a global LHC fit, the electron EDM and baryogenesis*, *Eur. Phys. J. C* **82**, 604 (2022), [arXiv:2202.11753 \[hep-ph\]](#).
- [103] G. Panico, A. Pomarol, and M. Riembau, *EFT approach to the electron Electric Dipole Moment at the two-loop level*, *JHEP* **04**, 090, [arXiv:1810.09413 \[hep-ph\]](#).
- [104] S. R. Coleman and E. J. Weinberg, *Radiative Corrections as the Origin of Spontaneous Symmetry Breaking*, *Phys. Rev. D* **7**, 1888 (1973).
- [105] G. W. Anderson and L. J. Hall, *The Electroweak phase transition and baryogenesis*, *Phys. Rev. D* **45**, 2685 (1992).
- [106] M. Quiros, in *ICTP Summer School in High-Energy Physics and Cosmology* (1999) pp. 187–259, [arXiv:hep-ph/9901312](#).
- [107] P. B. Arnold and O. Espinosa, *The Effective potential and first order phase transitions: Beyond leading-order*, *Phys. Rev. D* **47**, 3546 (1993), [Erratum: *Phys. Rev. D* 50, 6662 (1994)], [arXiv:hep-ph/9212235](#).
- [108] S. R. Coleman, *The Fate of the False Vacuum. 1. Semi-classical Theory*, *Phys. Rev. D* **15**, 2929 (1977), [Erratum: *Phys. Rev. D* 16, 1248 (1977)].
- [109] J. Callan, Curtis G. and S. R. Coleman, *The Fate of the False Vacuum. 2. First Quantum Corrections*, *Phys. Rev. D* **16**, 1762 (1977).
- [110] C. Caprini *et al.*, *Detecting gravitational waves from cosmological phase transitions with LISA: an update*, *JCAP* **03**, 024, [arXiv:1910.13125 \[astro-ph.CO\]](#).
- [111] C. L. Wainwright, *CosmoTransitions: Computing Cosmological Phase Transition Temperatures and Bubble Profiles with Multiple Fields*, *Comput. Phys. Commun.* **183**, 2006 (2012), [arXiv:1109.4189 \[hep-ph\]](#).
- [112] P. Auclair *et al.* (LISA Cosmology Working Group), *Cosmology with the Laser Interferometer Space Antenna*, *Living Rev. Rel.* **26**, 5 (2023), [arXiv:2204.05434 \[astro-ph.CO\]](#).
- [113] A. Ekstedt, O. Gould, J. Hirvonen, B. Laurent, L. Niemi, P. Schicho, and J. van de Vis, *How fast does the WallGo? A package for computing wall velocities in first-order phase transitions*, *JHEP* **04**, 101, [arXiv:2411.04970 \[hep-ph\]](#).
- [114] H. H. Patel and M. J. Ramsey-Musolf, *Baryon Washout, Electroweak Phase Transition, and Perturbation Theory*, *JHEP* **07**, 029, [arXiv:1101.4665 \[hep-ph\]](#).
- [115] M. Garny and T. Konstandin, *On the gauge dependence of vacuum transitions at finite temperature*, *JHEP* **07**, 189, [arXiv:1205.3392 \[hep-ph\]](#).
- [116] L. Fromme and S. J. Huber, *Top transport in electroweak baryogenesis*, *JHEP* **03**, 049, [arXiv:hep-ph/0604159](#).
- [117] M. Joyce, T. Prokopec, and N. Turok, *Electroweak baryogenesis from a classical force*, *Phys. Rev. Lett.* **75**, 1695 (1995), [Erratum: *Phys. Rev. Lett.* 75, 3375 (1995)], [arXiv:hep-ph/9408339](#).

- [118] M. Joyce, T. Prokopec, and N. Turok, *Nonlocal electroweak baryogenesis. Part 2: The Classical regime*, *Phys. Rev. D* **53**, 2958 (1996), [arXiv:hep-ph/9410282](#).
- [119] J. M. Cline and K. Kainulainen, *Electroweak baryogenesis at high bubble wall velocities*, *Phys. Rev. D* **101**, 063525 (2020), [arXiv:2001.00568 \[hep-ph\]](#).
- [120] E. Witten, *Cosmic Separation of Phases*, *Phys. Rev. D* **30**, 272 (1984).
- [121] C. J. Hogan, *Gravitational radiation from cosmological phase transitions*, *Mon. Not. Roy. Astron. Soc.* **218**, 629 (1986).
- [122] P. Amaro-Seoane *et al.* (LISA), *Laser Interferometer Space Antenna*, (2017), [arXiv:1702.00786 \[astro-ph.IM\]](#).
- [123] P. Auclair *et al.* (LISA Cosmology Working Group), *Cosmology with the Laser Interferometer Space Antenna*, *Living Rev. Rel.* **26**, 5 (2023), [arXiv:2204.05434 \[astro-ph.CO\]](#).
- [124] P. Auclair, C. Caprini, D. Cutting, M. Hindmarsh, K. Rummukainen, D. A. Steer, and D. J. Weir, *Generation of gravitational waves from freely decaying turbulence*, (2022), [arXiv:2205.02588 \[astro-ph.CO\]](#).
- [125] *LISA: Science Requirements Document*, Tech. Rep. *ESA-L3-EST-SCI-RS-001* (2018).
- [126] M. Postma, J. van de Vis, and G. White, *Resummation and cancellation of the VIA source in electroweak baryogenesis*, *JHEP* **12**, 121, [arXiv:2206.01120 \[hep-ph\]](#).
- [127] T. Krajewski, M. Lewicki, I. Nalecz, and M. Zych, *Steady-state bubbles beyond local thermal equilibrium*, (2024), [arXiv:2411.16580 \[astro-ph.CO\]](#).
- [128] D. Curtin, P. Meade, and H. Ramani, *Thermal Resummation and Phase Transitions*, *Eur. Phys. J. C* **78**, 787 (2018), [arXiv:1612.00466 \[hep-ph\]](#).
- [129] G. Aad *et al.* (ATLAS), *Search for a CP-odd Higgs boson decaying into a heavy CP-even Higgs boson and a Z boson in the $\ell^+\ell^-\bar{t}t$ and $\nu\bar{\nu}b\bar{b}$ final states using 140 fb $^{-1}$ of data collected with the ATLAS detector*, *JHEP* **02**, 197, [arXiv:2311.04033 \[hep-ex\]](#).
- [130] A. Hayrapetyan *et al.* (CMS), *Search for heavy neutral Higgs bosons A and H in the $t\bar{t}Z$ channel in proton-proton collisions at 13 TeV*, (2024), [arXiv:2412.00570 \[hep-ex\]](#).
- [131] A. Hayrapetyan *et al.* (CMS), *Searches for Higgs boson production through decays of heavy resonances*, *Phys. Rept.* **1115**, 368 (2025), [arXiv:2403.16926 \[hep-ex\]](#).
- [132] A. Tumasyan *et al.* (CMS), *A portrait of the Higgs boson by the CMS experiment ten years after the discovery*, *Nature* **607**, 60 (2022), [arXiv:2207.00043 \[hep-ex\]](#).
- [133] *A detailed map of Higgs boson interactions by the ATLAS experiment ten years after the discovery*, *Nature* **607**, 52 (2022), [Erratum: *Nature* 612, E24 (2022)], [arXiv:2207.00092 \[hep-ex\]](#).
- [134] G. Aad *et al.* (ATLAS), *Search for heavy neutral Higgs bosons decaying into a top quark pair in 140 fb $^{-1}$ of proton-proton collision data at $\sqrt{s} = 13$ TeV with the ATLAS detector*, *JHEP* **08**, 013, [arXiv:2404.18986 \[hep-ex\]](#).
- [135] *Search for heavy pseudoscalar and scalar bosons decaying to top quark pairs in proton-proton collisions at $\sqrt{s} = 13$ TeV*, Tech. Rep. *CMS-PAS-HIG-22-013* (CERN, Geneva, 2024).
- [136] G. Aad *et al.* (ATLAS), *Search for charged Higgs bosons decaying into a top quark and a bottom quark at $\sqrt{s} = 13$ TeV with the ATLAS detector*, *JHEP* **06**, 145, [arXiv:2102.10076 \[hep-ex\]](#).
- [137] A. Tumasyan *et al.* (CMS), *Search for a scalar or pseudoscalar dilepton resonance produced in association with a massive vector boson or top quark-antiquark pair in multilepton events at $s=13$ TeV*, *Phys. Rev. D* **110**, 012013 (2024), [arXiv:2402.11098 \[hep-ex\]](#).
- [138] G. Aad *et al.* (ATLAS), *Search for heavy Higgs bosons decaying into two tau leptons with the ATLAS detector using pp collisions at $\sqrt{s} = 13$ TeV*, *Phys. Rev. Lett.* **125**, 051801 (2020), [arXiv:2002.12223 \[hep-ex\]](#).
- [139] M. Aaboud *et al.* (ATLAS), *Search for heavy resonances decaying into WW in the $e\nu\mu\nu$ final state in pp collisions at $\sqrt{s} = 13$ TeV with the ATLAS detector*, *Eur. Phys. J. C* **78**, 24 (2018), [arXiv:1710.01123 \[hep-ex\]](#).
- [140] A. M. Sirunyan *et al.* (CMS), *Search for a heavy Higgs boson decaying to a pair of W bosons in proton-proton collisions at $\sqrt{s} = 13$ TeV*, *JHEP* **03**, 034, [arXiv:1912.01594 \[hep-ex\]](#).
- [141] A. M. Sirunyan *et al.* (CMS), *Search for a new scalar resonance decaying to a pair of Z bosons in proton-proton collisions at $\sqrt{s} = 13$ TeV*, *JHEP* **06**, 127, [Erratum: *JHEP* 03, 128 (2019)], [arXiv:1804.01939 \[hep-ex\]](#).
- [142] G. Aad *et al.* (ATLAS), *Search for heavy resonances decaying into a pair of Z bosons in the $\ell^+\ell^-\ell'^+\ell'^-$ and $\ell^+\ell^-\nu\bar{\nu}$ final states using 139 fb $^{-1}$ of proton-proton collisions at $\sqrt{s} = 13$ TeV with the ATLAS detector*, *Eur. Phys. J. C* **81**, 332 (2021), [arXiv:2009.14791 \[hep-ex\]](#).
- [143] A. Tumasyan *et al.* (CMS), *Searches for additional Higgs bosons and for vector leptoquarks in $\tau\tau$ final states in proton-proton collisions at $\sqrt{s} = 13$ TeV*, *JHEP* **07**, 073, [arXiv:2208.02717 \[hep-ex\]](#).
- [144] G. Aad *et al.* (ATLAS), *Search for resonances decaying into photon pairs in 139 fb $^{-1}$ of pp collisions at $\sqrt{s}=13$ TeV with the ATLAS detector*, *Phys. Lett. B* **822**, 136651 (2021), [arXiv:2102.13405 \[hep-ex\]](#).